Supplementary material

Ru-Based NSAIDs as Potential Anticancer Therapeutics

Silvia Bordoni*, Magda Monari, Carla Boga*, Federico Moro and Giacomo Drius

Contents

Characterization of **2**

IR spectrum

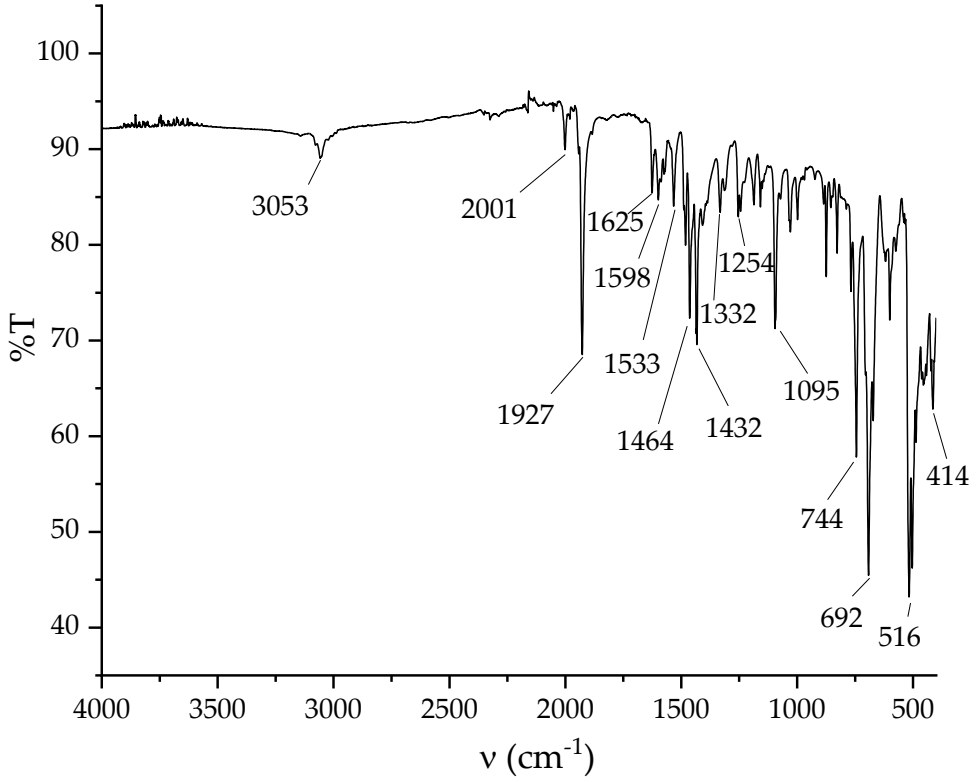

Figure S1. IR spectrum of **2.**

ESI-MS spectrum

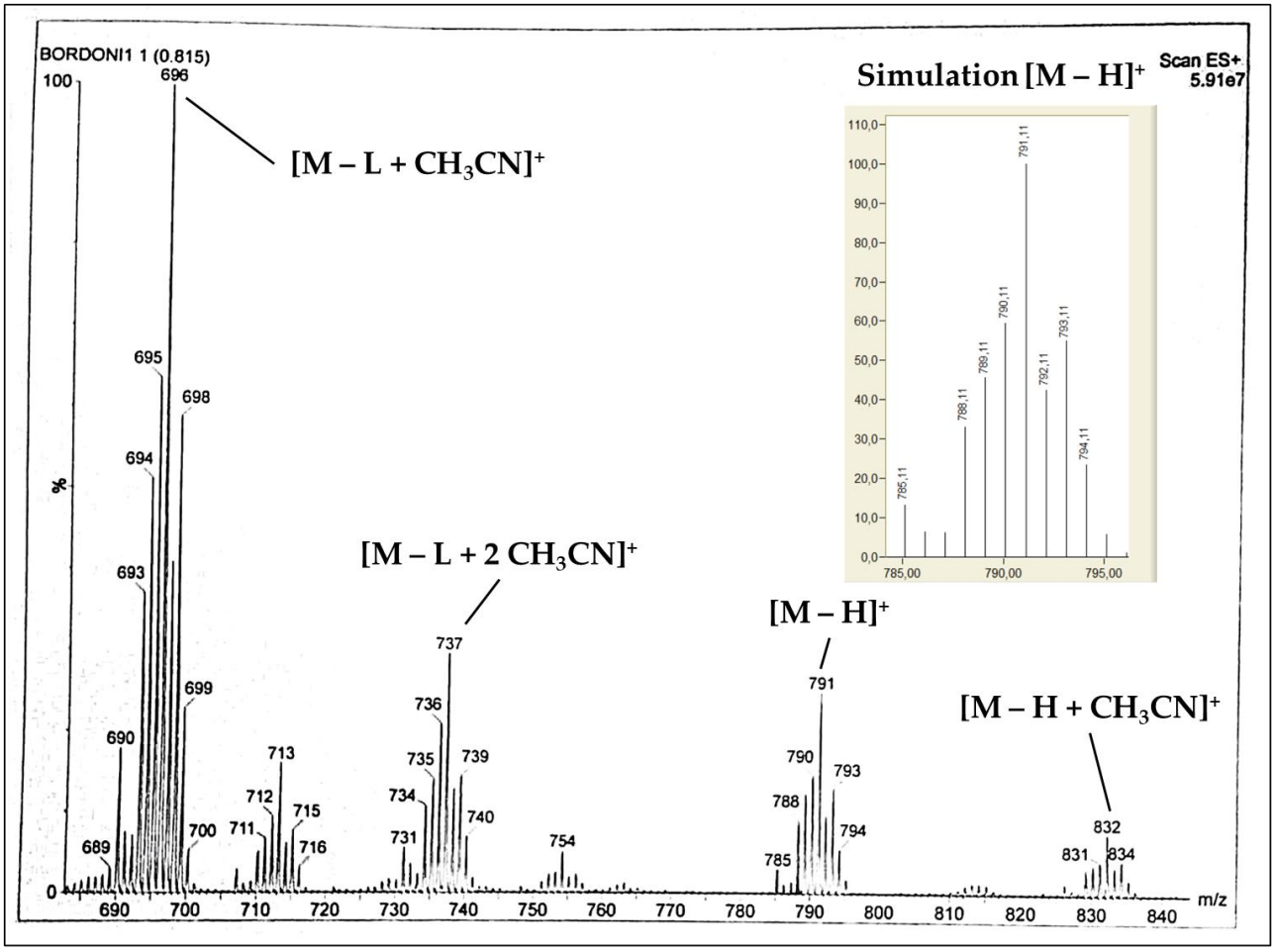

Figure S2. ESI-MS spectrum of **2** compared to simulation (positive mode, CH_3CN).

NMR spectra

^{1}H

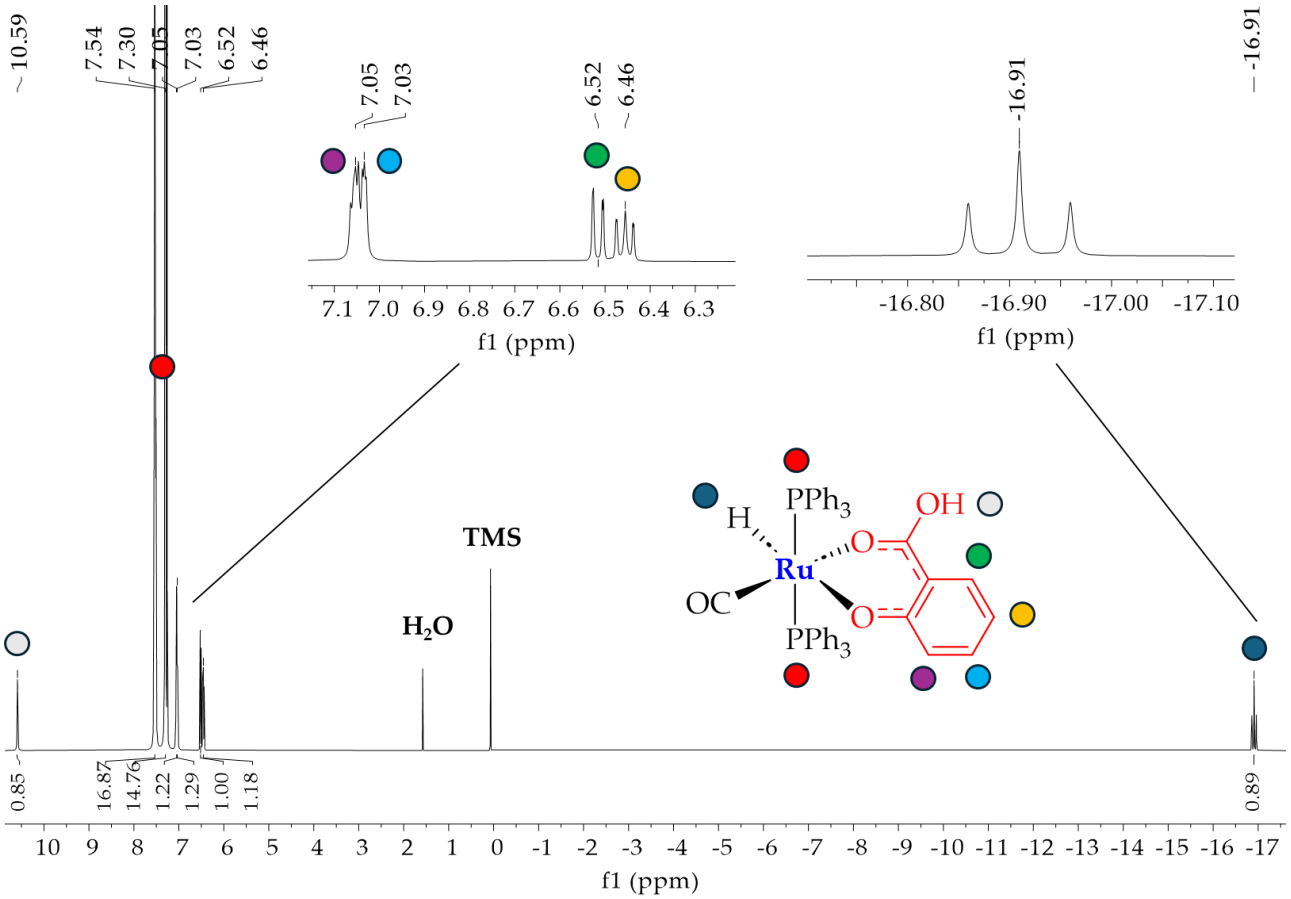

Figure S3. ^{1}H NMR of **2** ($CDCl_3$).

$^{31}P\{^{1}H\}$

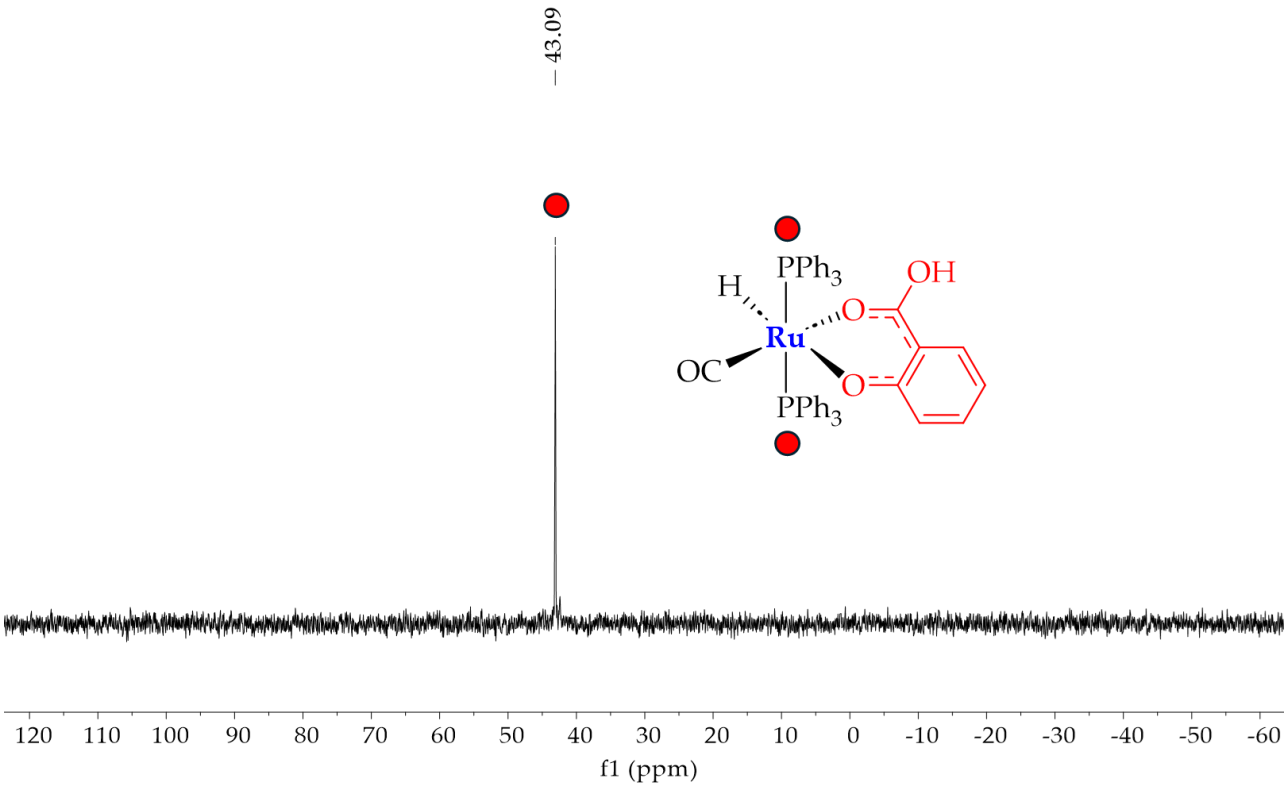

Figure S4. $^{31}P\{^{1}H\}$ NMR of **2** ($CDCl_3$).

$^{13}C\{^{1}H\}$

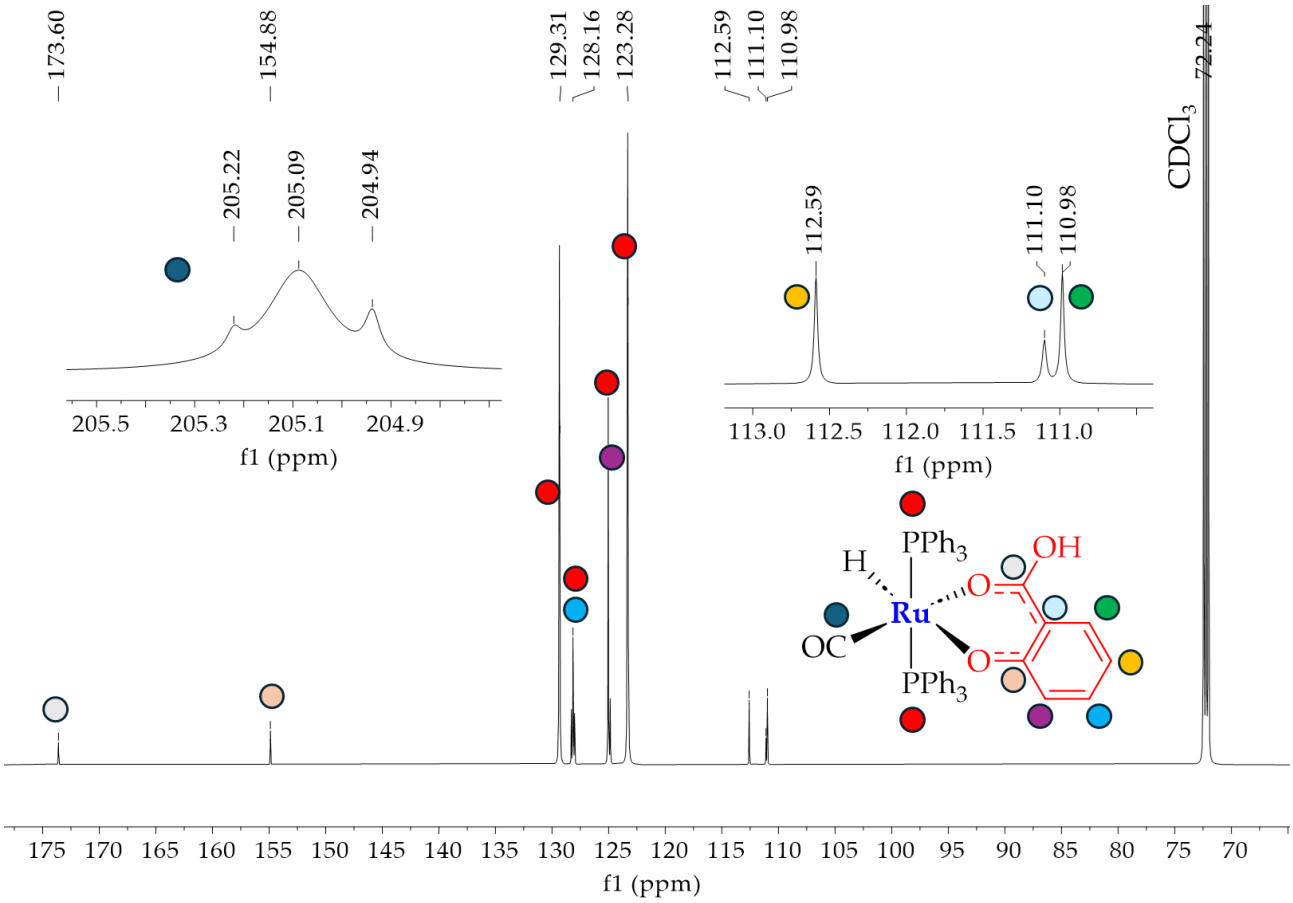

Figure S5. $^{13}C\{^{1}H\}$ NMR of **2** ($CDCl_3$).

HSQC

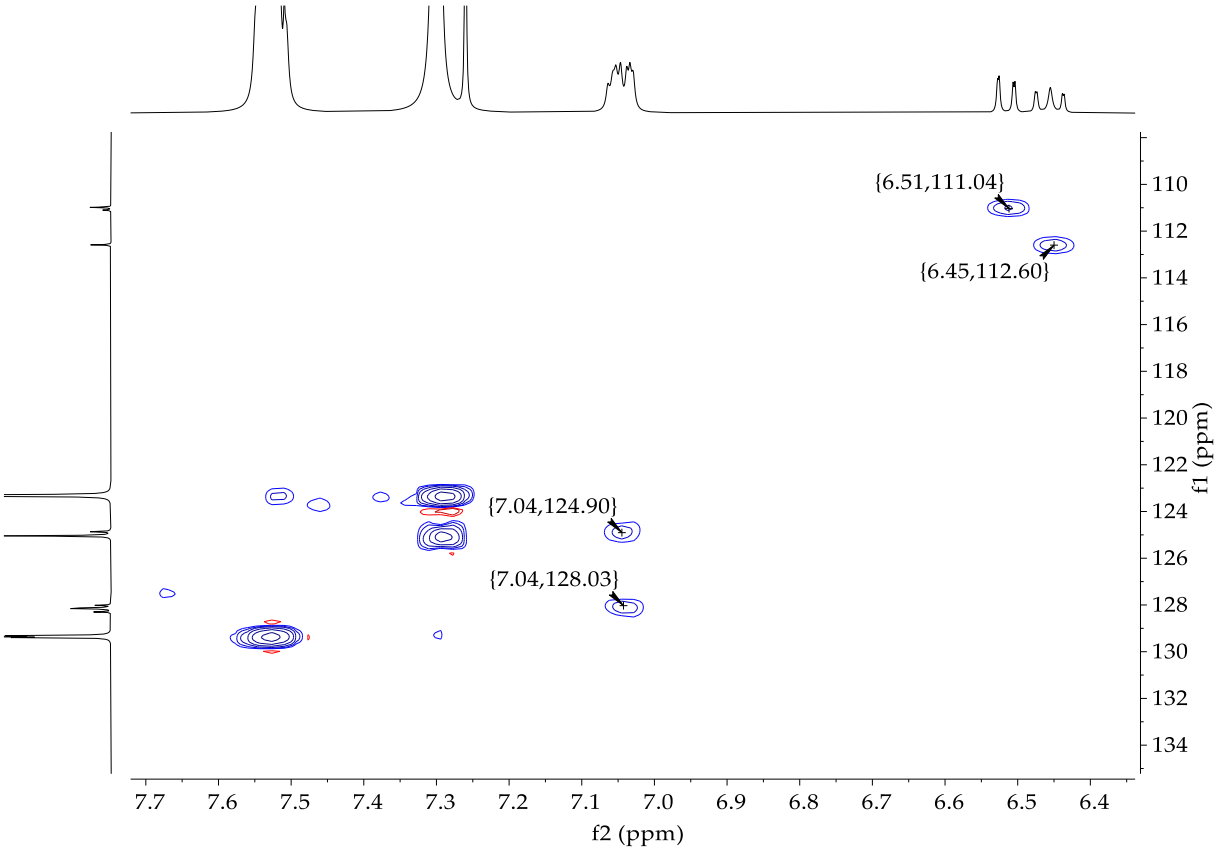

Figure S6. HSQC spectrum of **2.**

UV-Vis spectrum

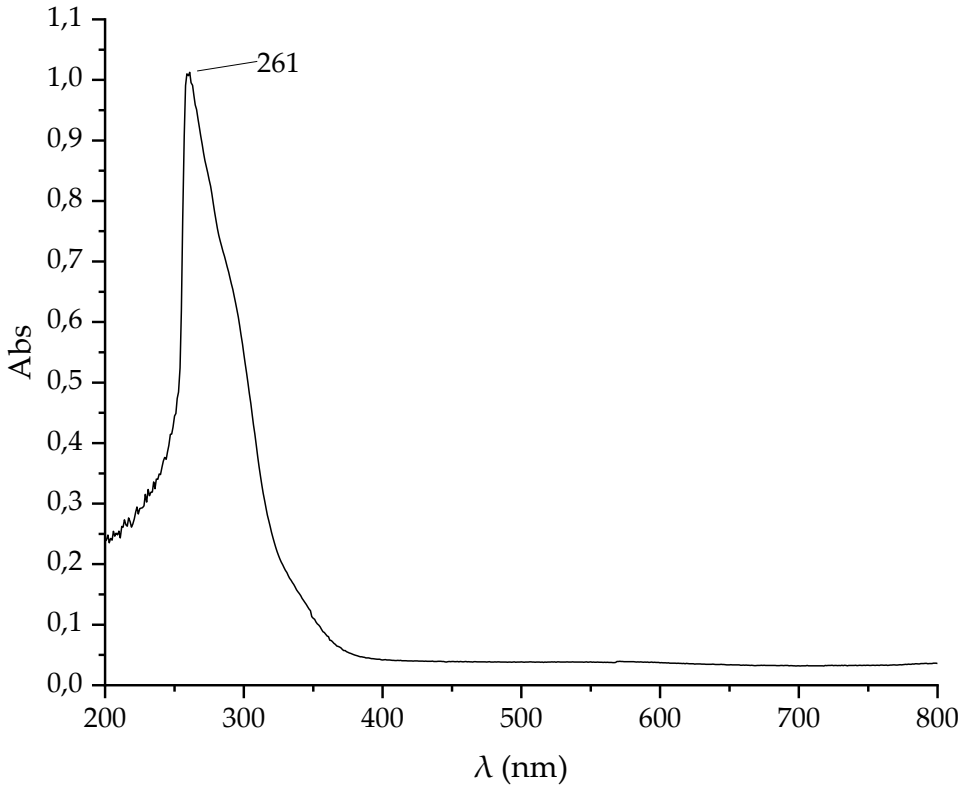

Figure S7. UV-Vis spectrum of **2** (DMSO, $1x10^{-5}$ M).

Stability test of **2** through UV-Vis spectroscopy

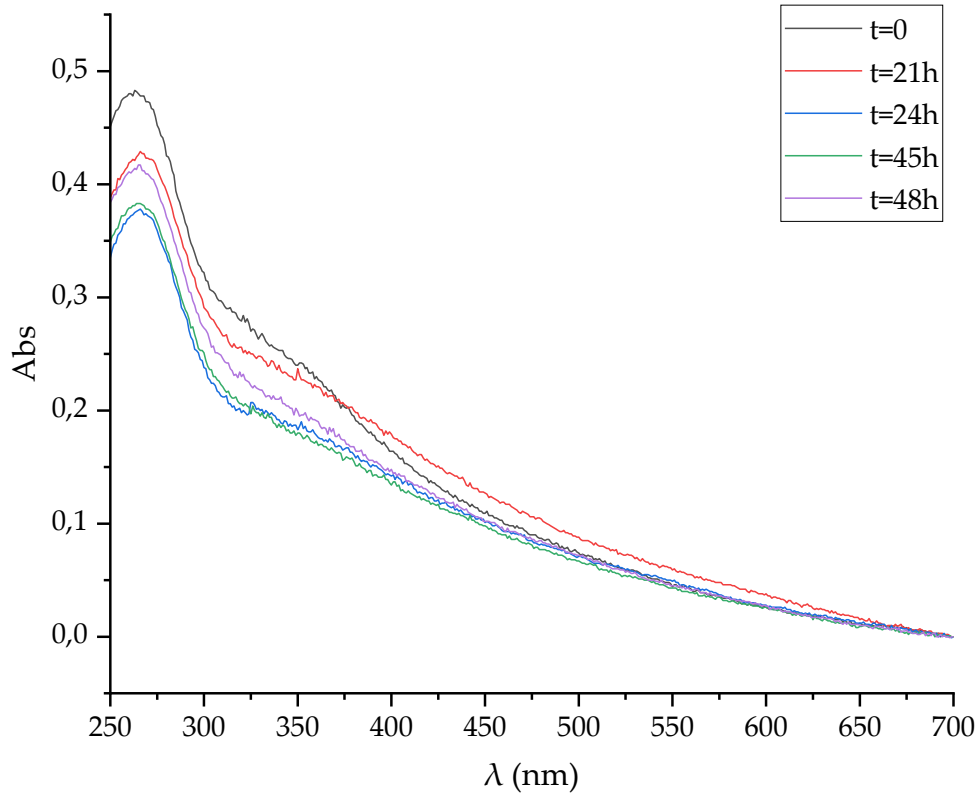

Figure S8. UV-Vis spectra of **2** in PBS-5% DMSO recorded over a period of 48 h.

Characterization of **3**

IR spectrum

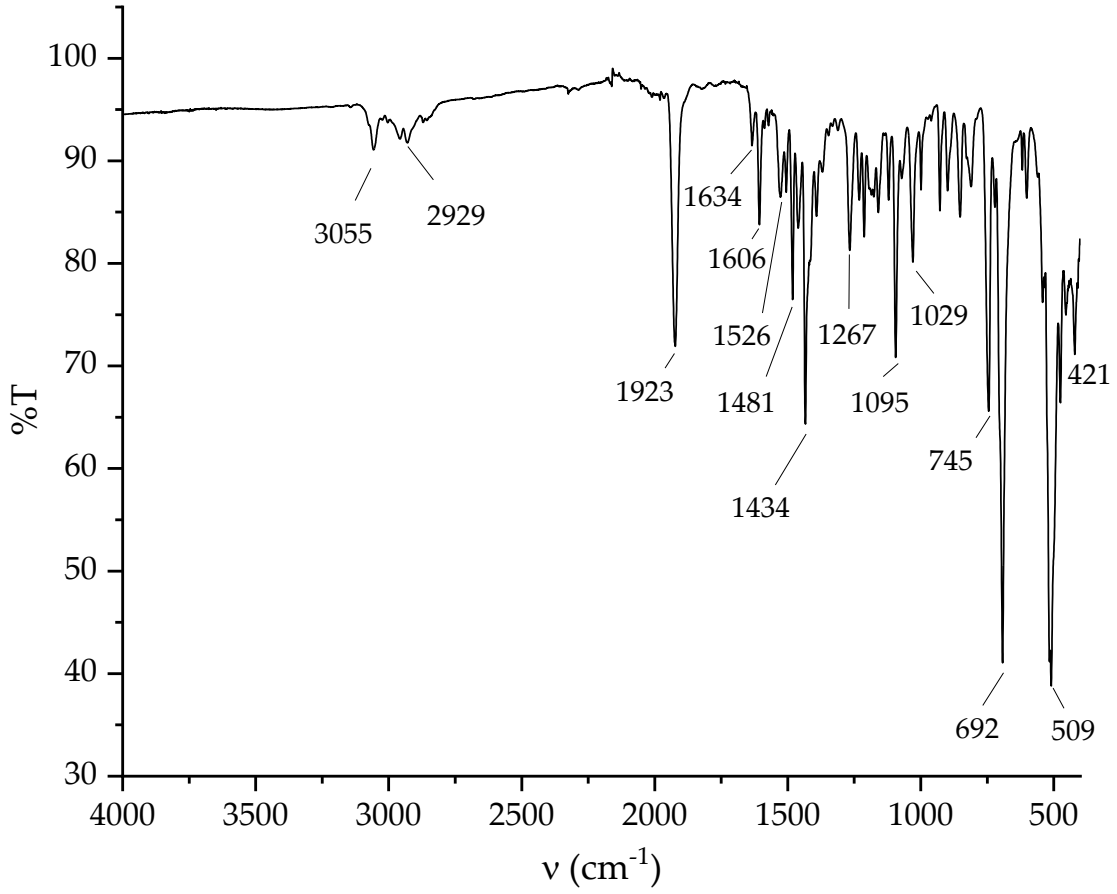

Figure S9. IR spectrum of **3**.

ESI-MS spectrum

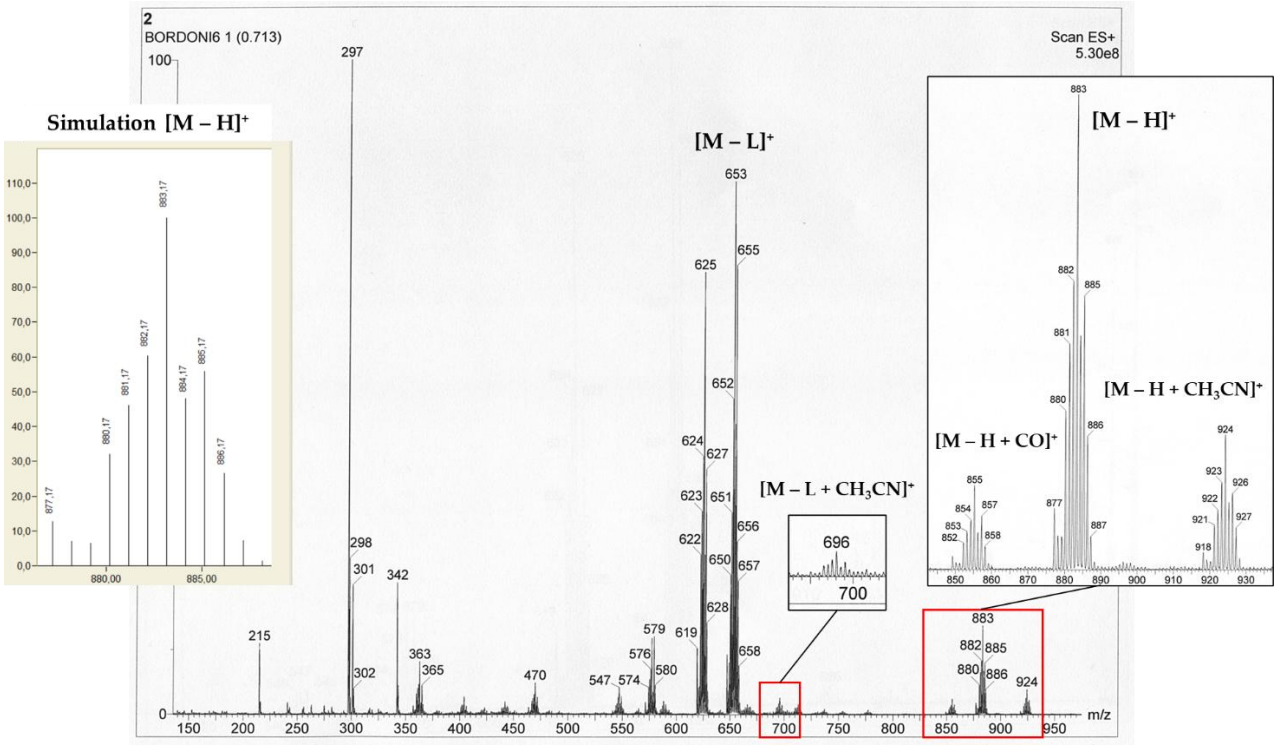

Figure S10. ESI-MS spectrum of **3** compared to simulation (positive mode, CH_3CN).

NMR spectra

^{1}H

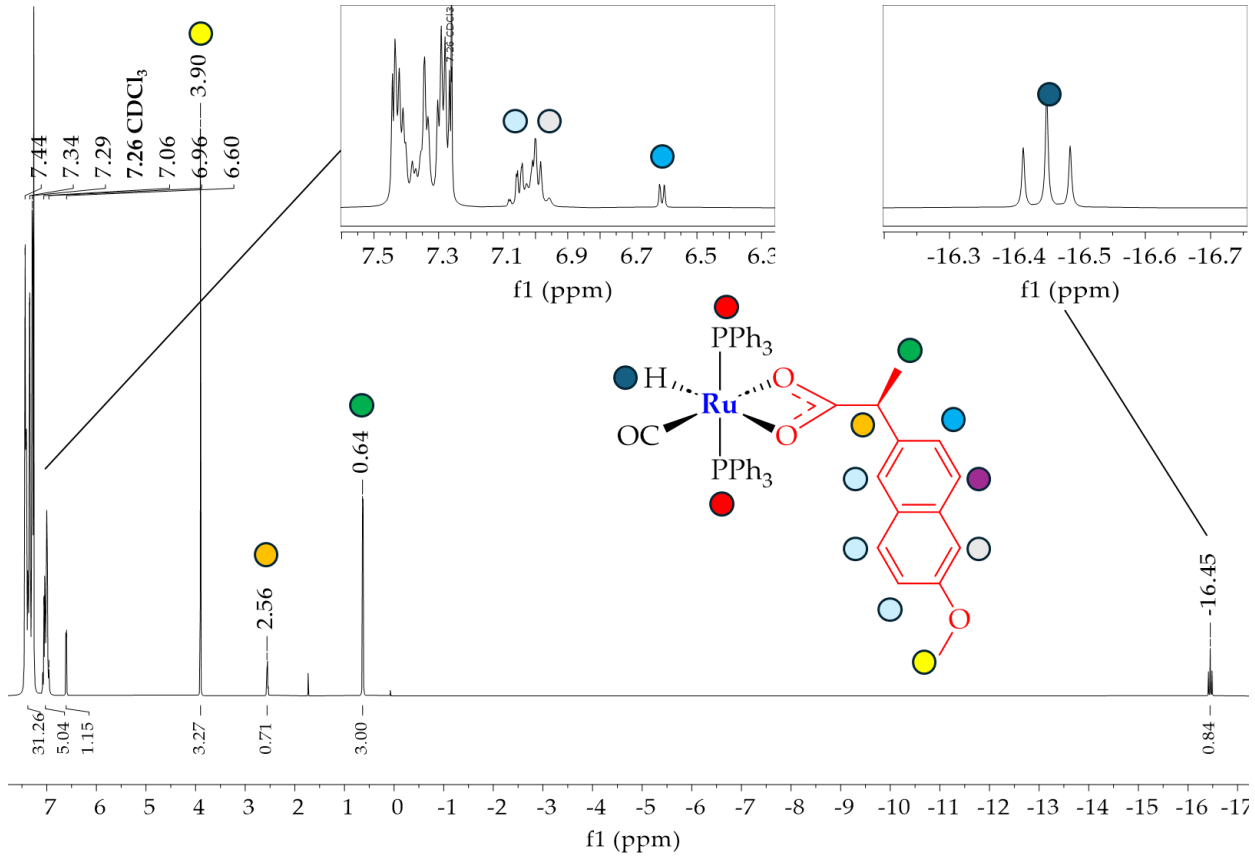

Figure S11. ^{1}H NMR spectrum of **3** ($CDCl_3$).

$^{31}P\{^{1}H\}$

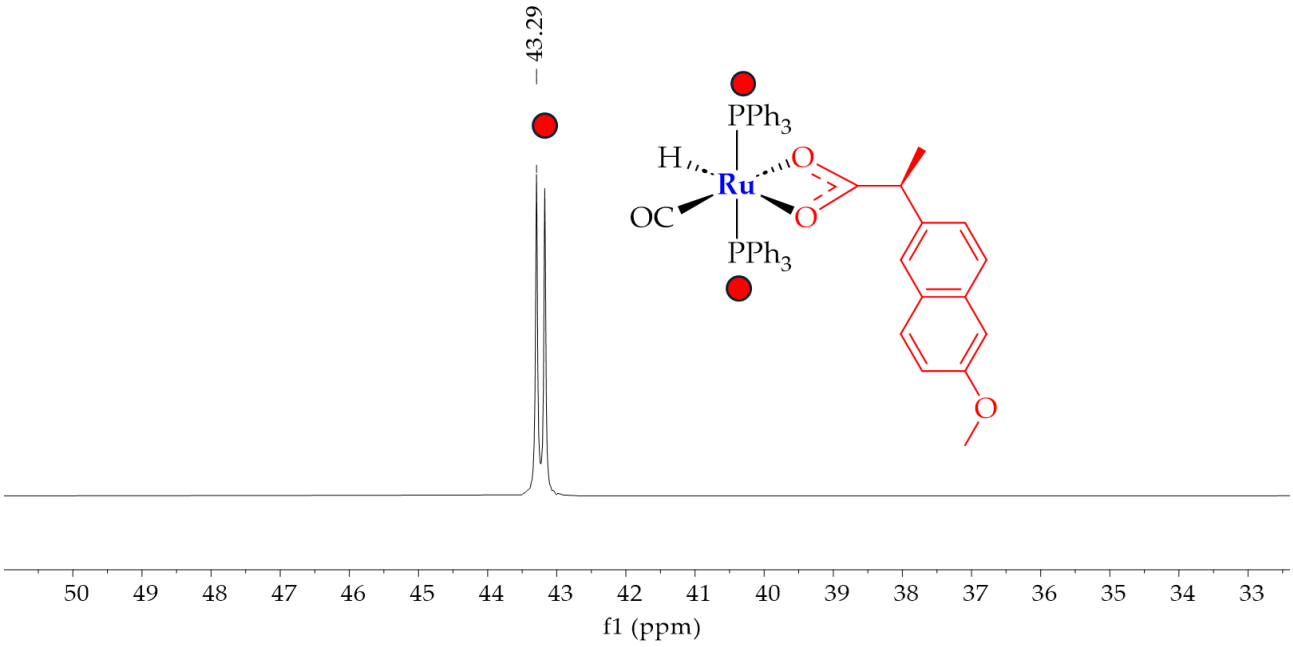

Figure S12. $^{31}P\{^{1}H\}$ NMR of **3** ($CDCl_3$).

$^{13}C\{^{1}H\}$

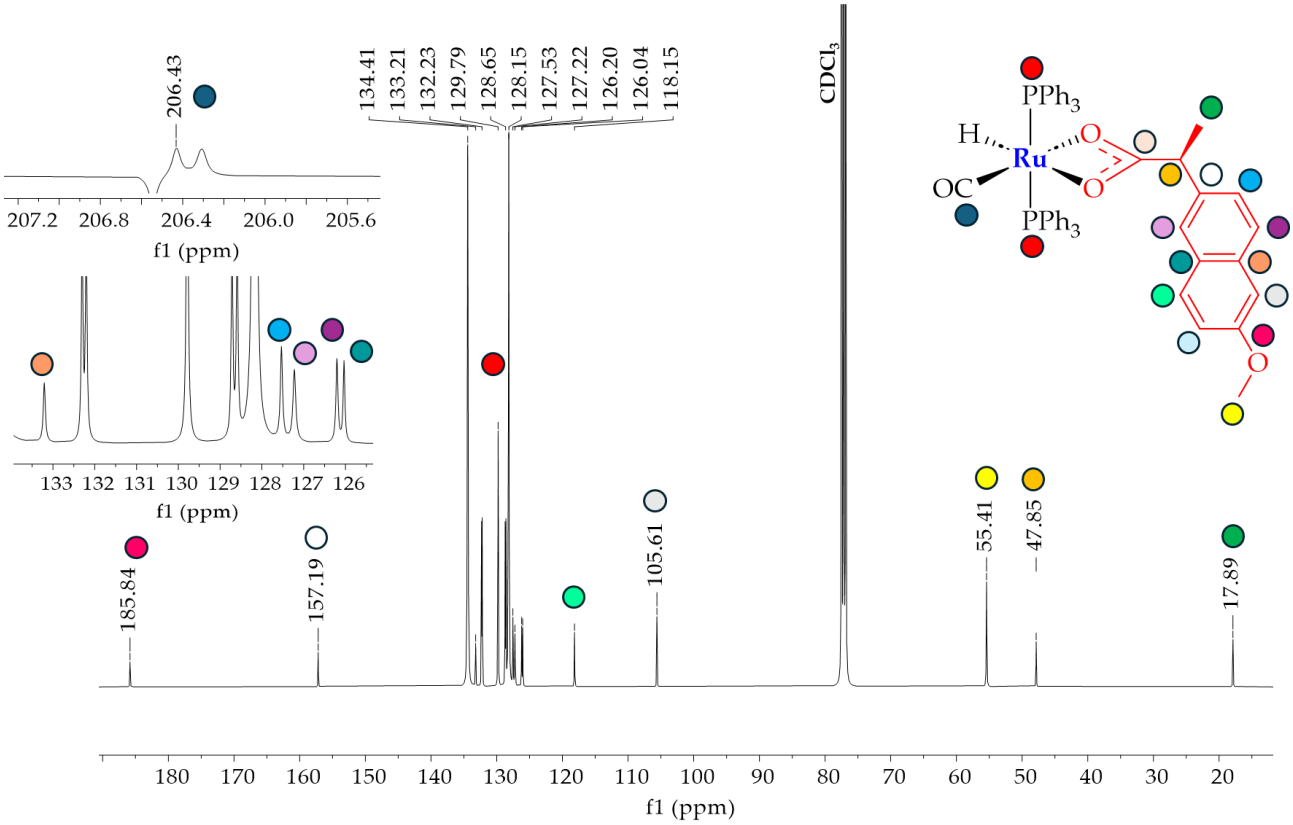

Figure S13. $^{13}C\{^{1}H\}$ NMR of **3** ($CDCl_3$).

HSQC

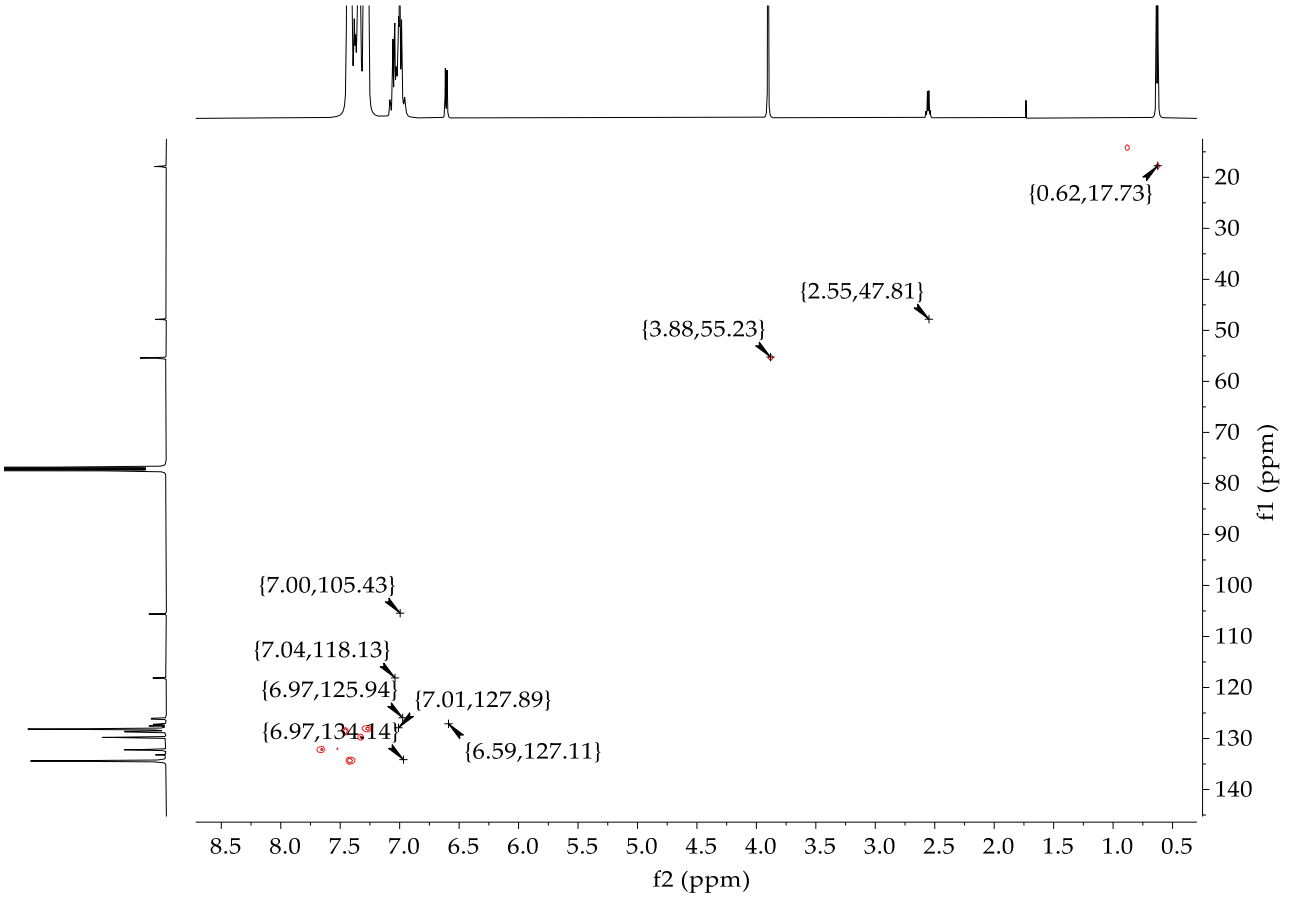

Figure S14. HSQC spectrum of **3** ($CDCl_3$).

HMBC

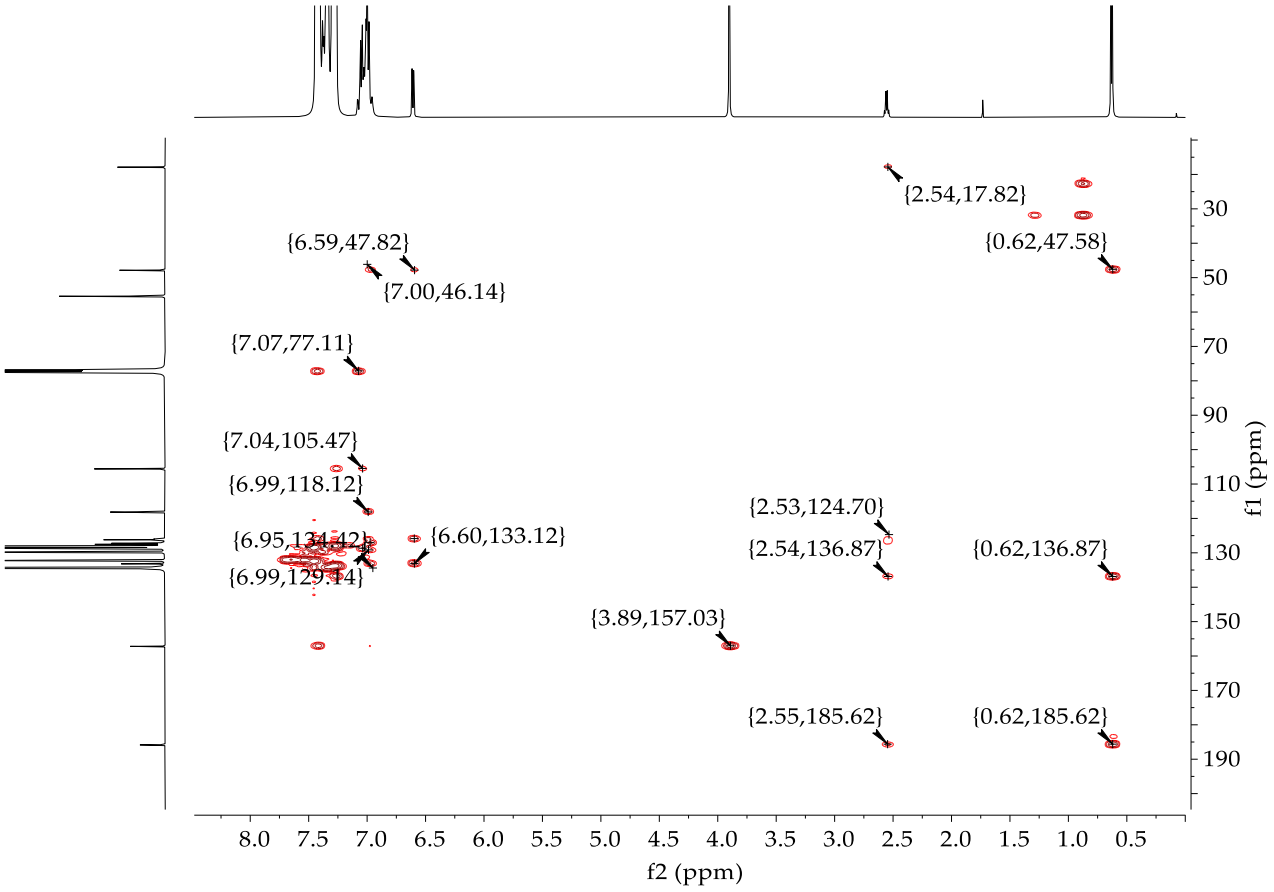

Figure S15. HMBC spectrum of **3** ($CDCl_3$).

UV-Vis spectrum

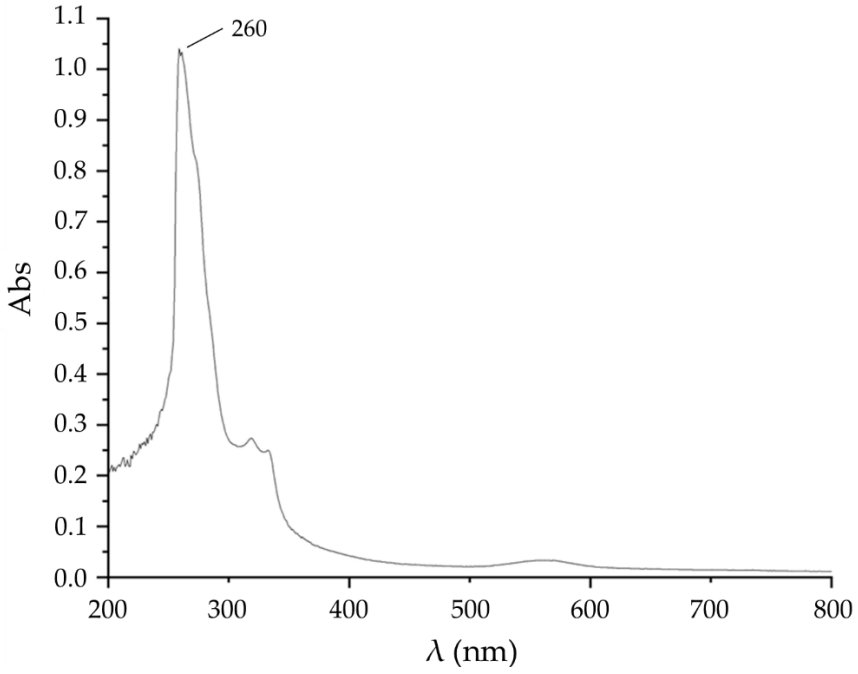

Figure S16. UV-Vis spectrum of **3** ($1x10^{-5}$ M, DMSO).

Characterization of **4**

IR spectrum

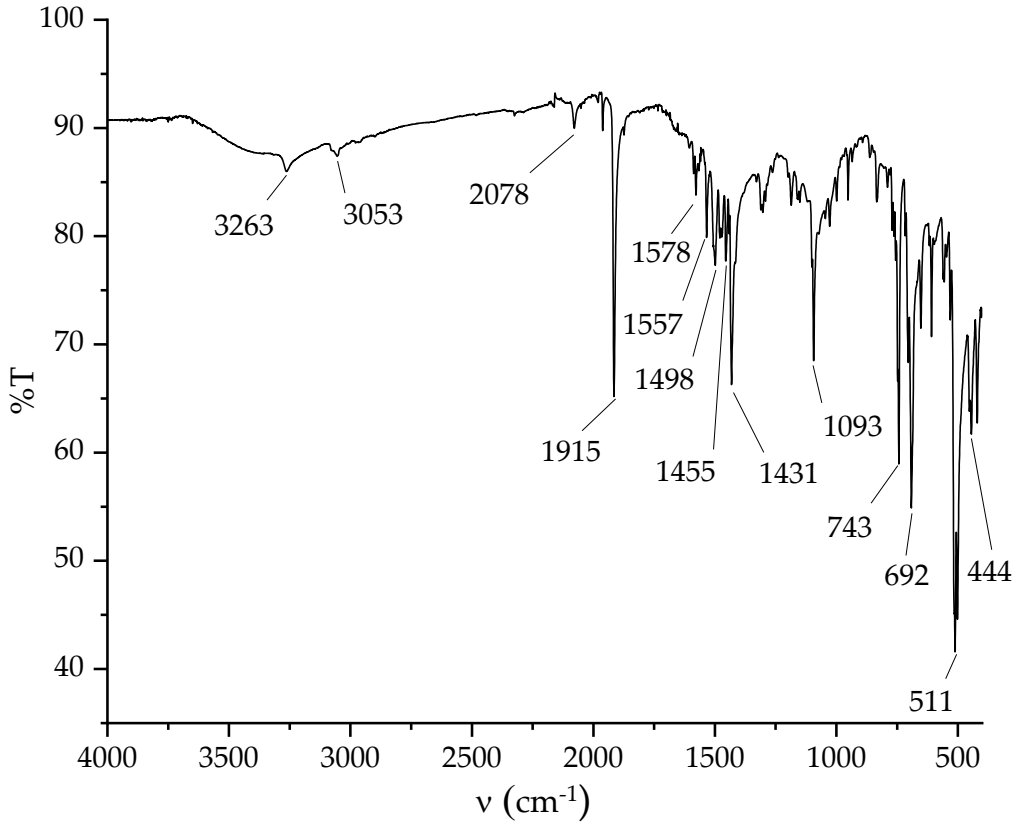

Figure S17. IR spectrum of **4**.

ESI-MS spectrum

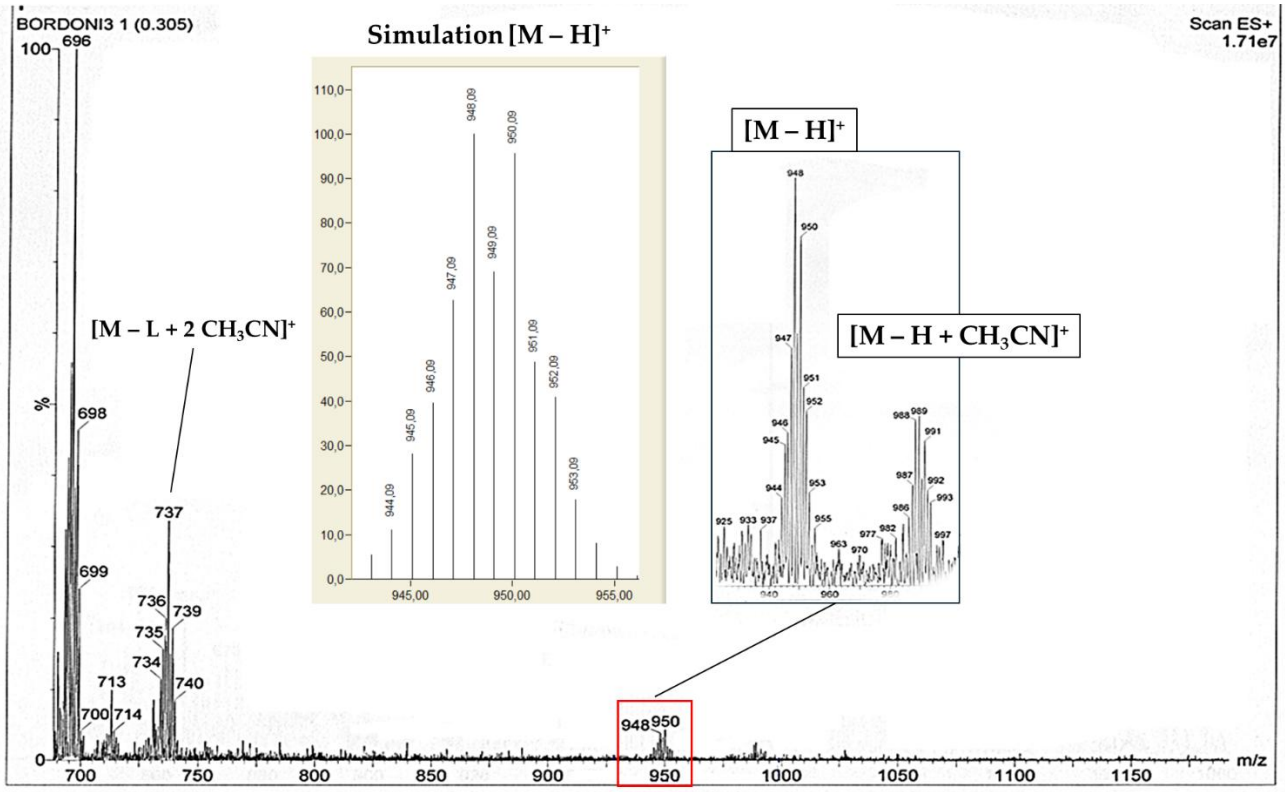

Figure S18. ESI-MS spectrum of **4** compared to simulation (positive mode, CH_3CN).

NMR spectra

^{1}H

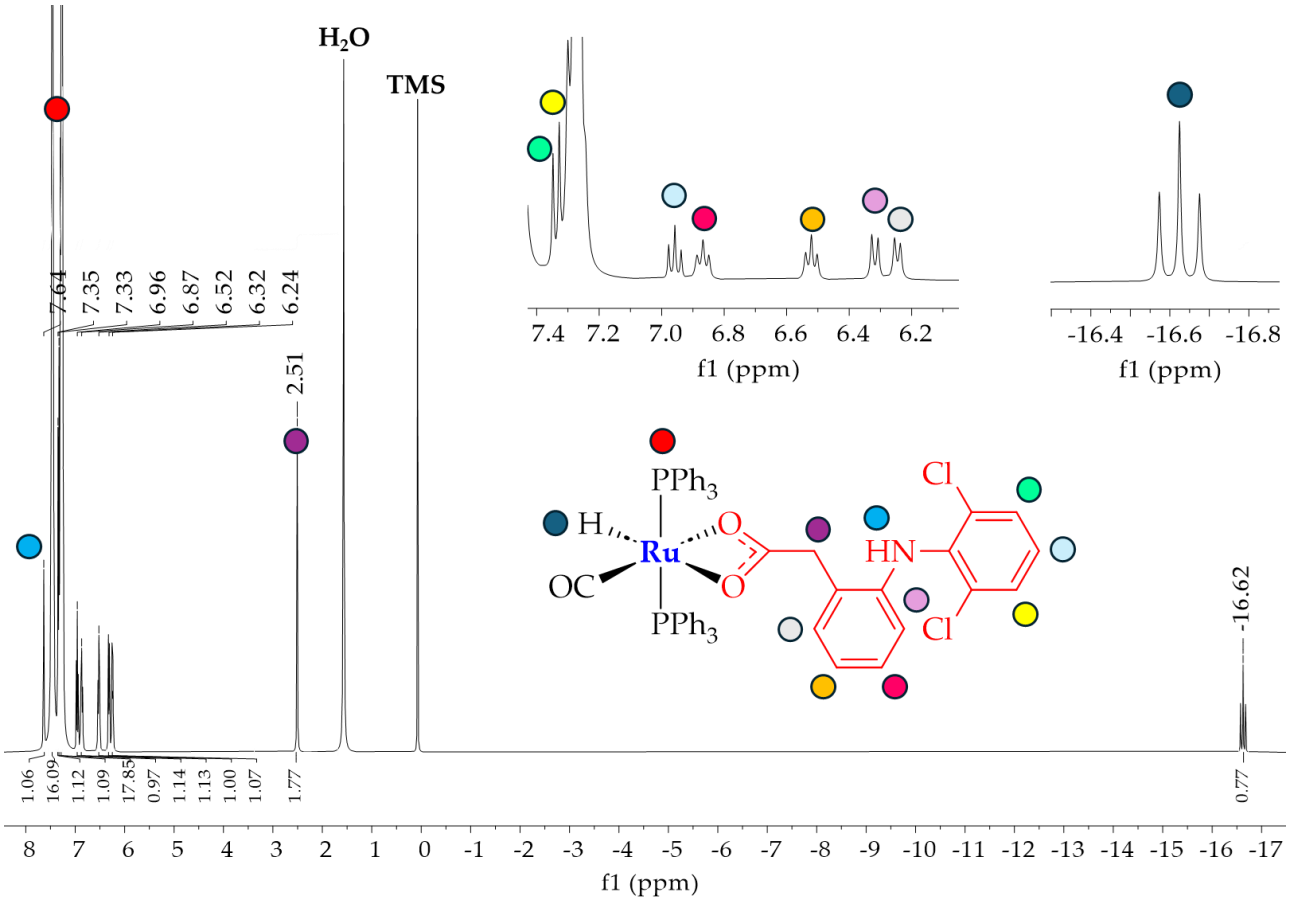

Figure S19. ^{1}H NMR spectrum of **4** ($CDCl_3$).

$^{31}P\{^{1}H\}$

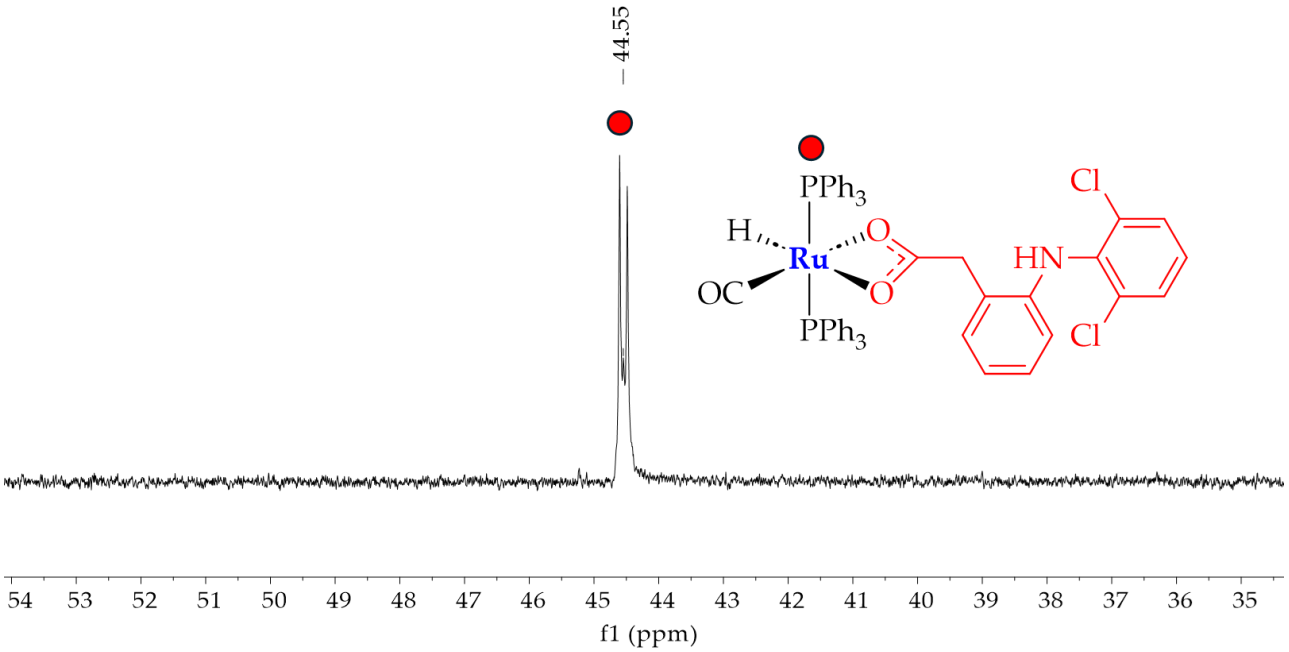

Figure S20: $^{31}P\{^{1}H\}$ NMR spectrum of **4** ($CDCl_3$).

$^{13}C\{^{1}H\}$

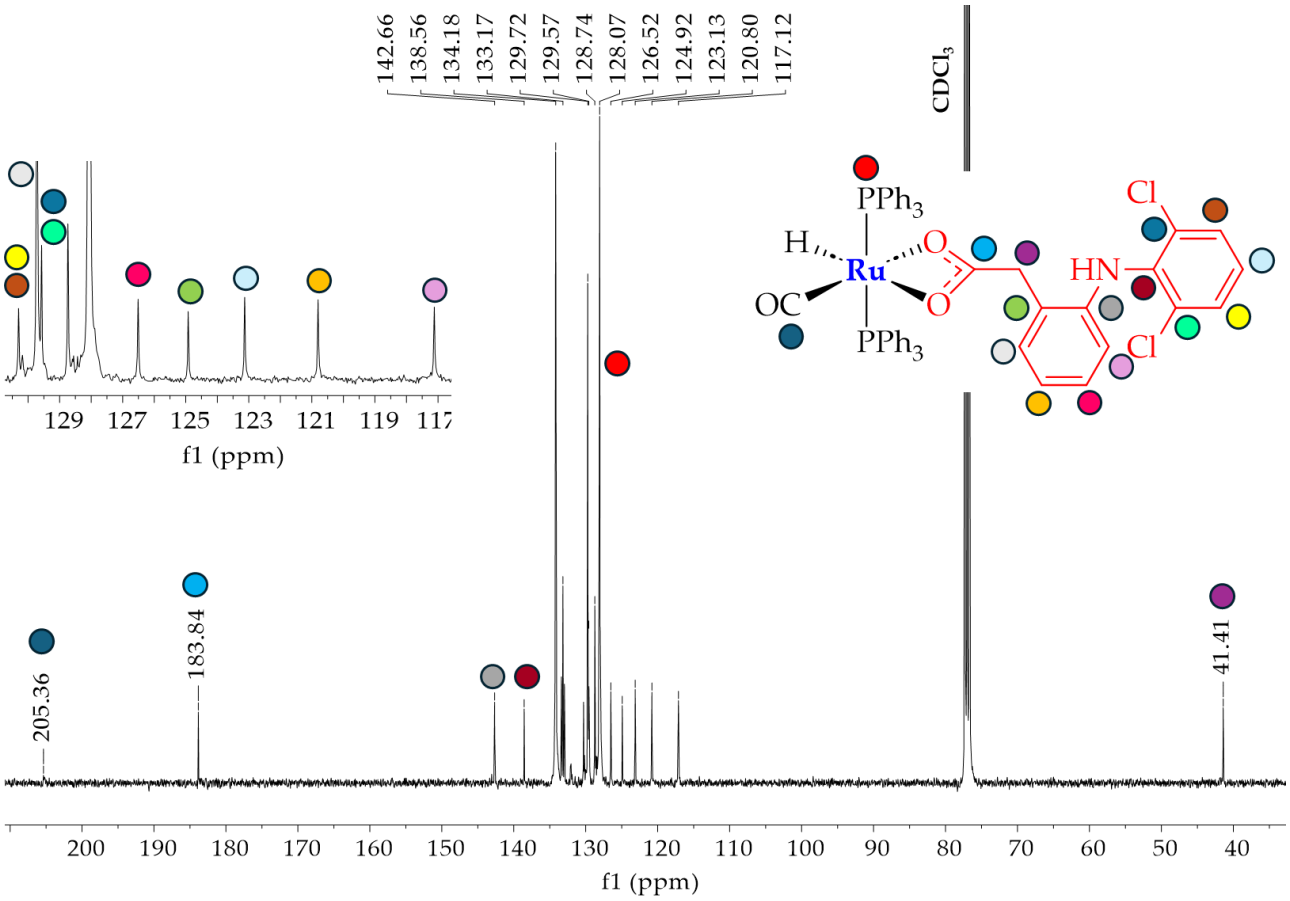

Figure S21. $^{13}C\{^{1}H\}$ spectrum of **4** ($CDCl_3$).

HSQC

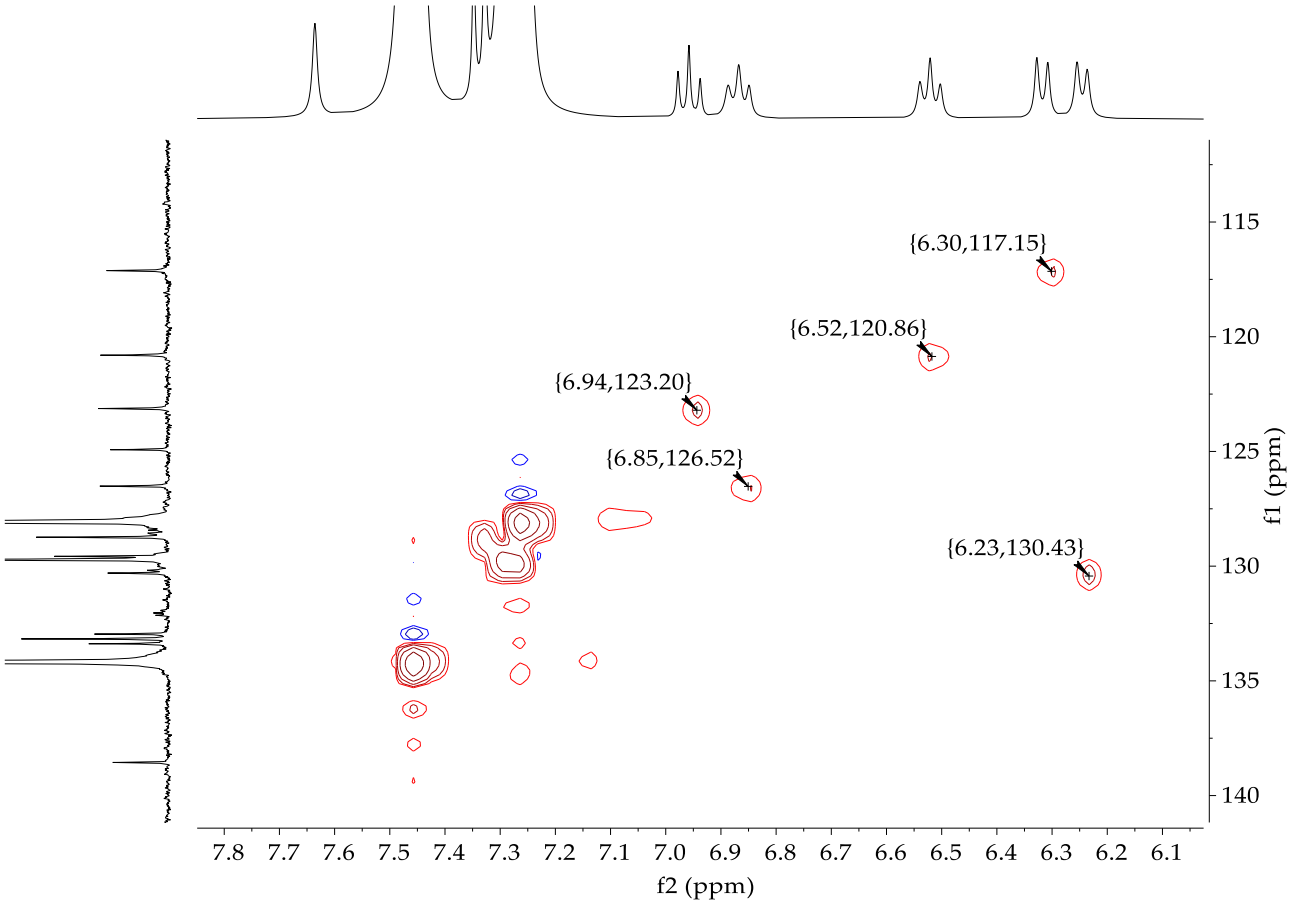

Figure S22. HSQC spectrum of **4** ($CDCl_3$).

HMBC

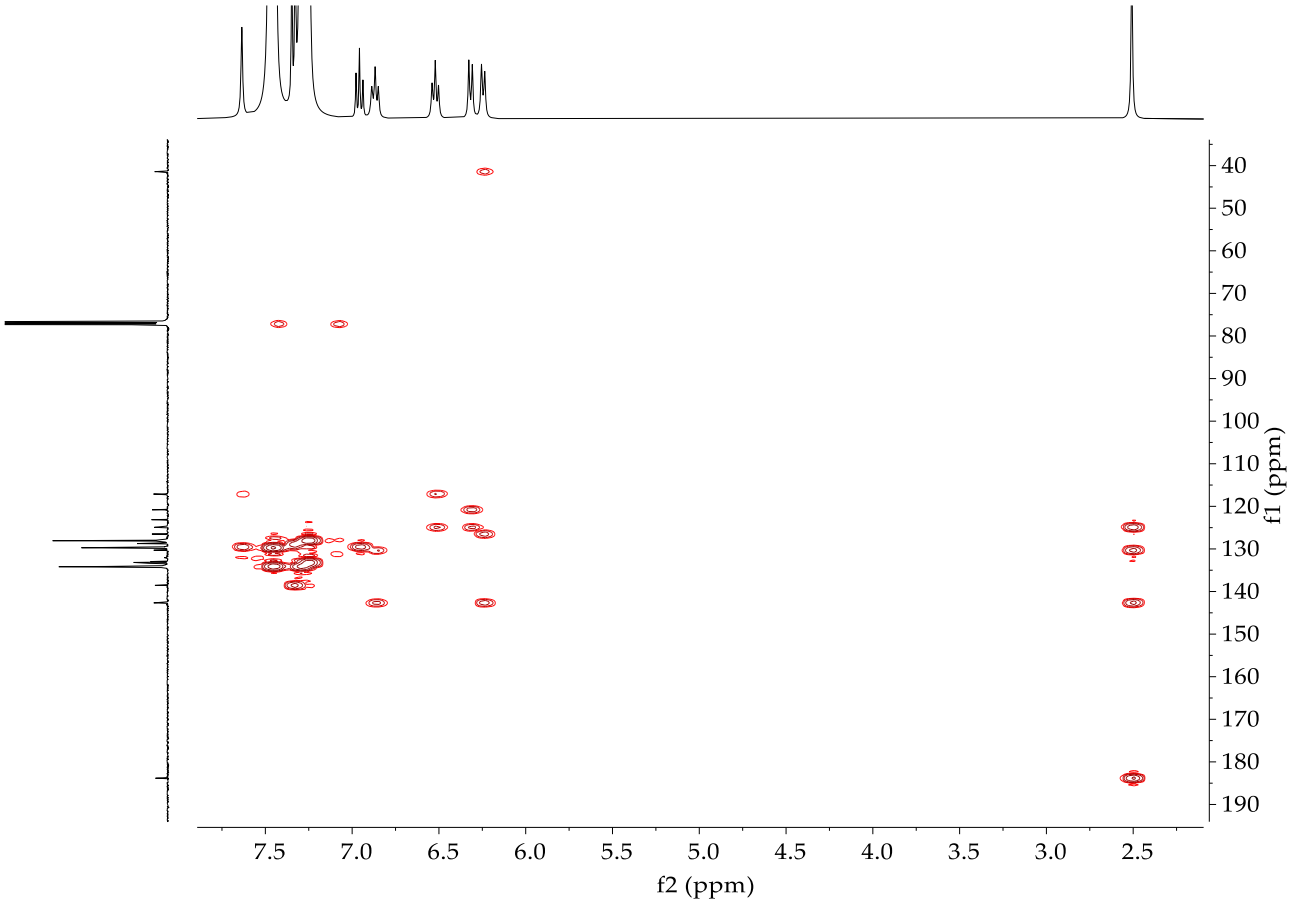

Figure S23. HMBC spectrum of **4** ($CDCl_3$).

UV-Vis spectrum

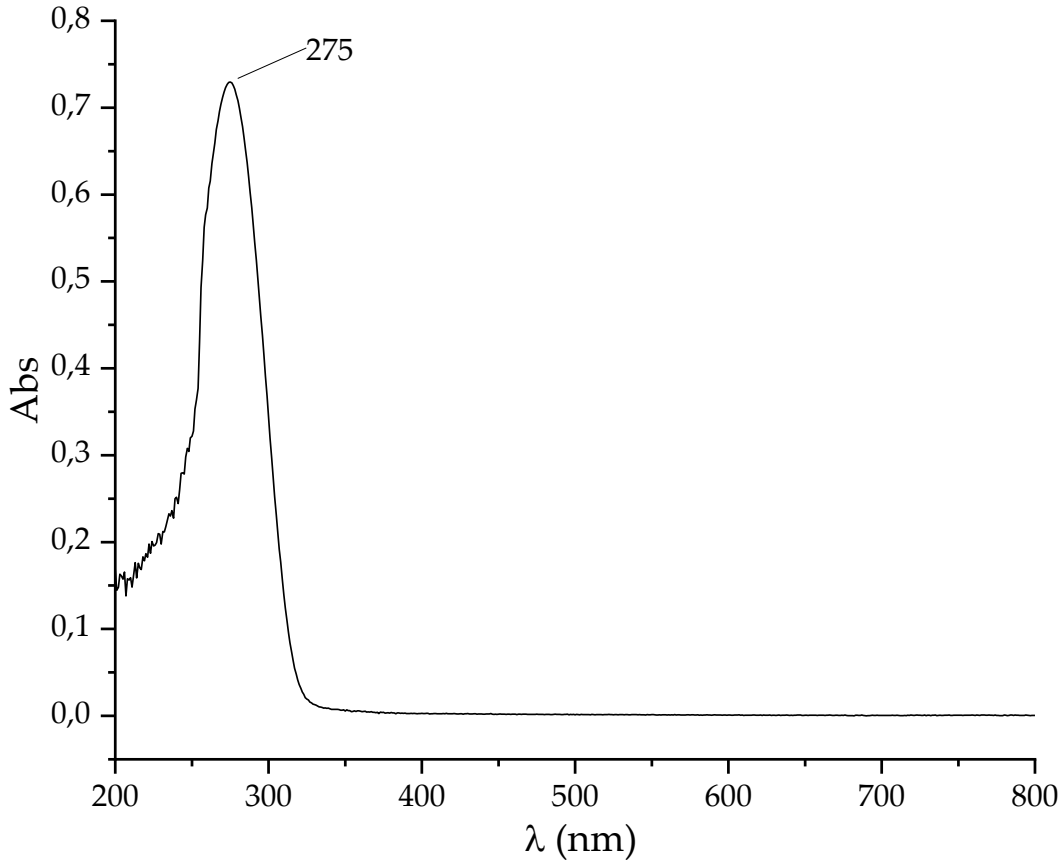

Figure S24. UV-Vis spectrum of **4** ($1x10^{-5}$ M, DMSO).

Characterization of **5**

IR spectrum

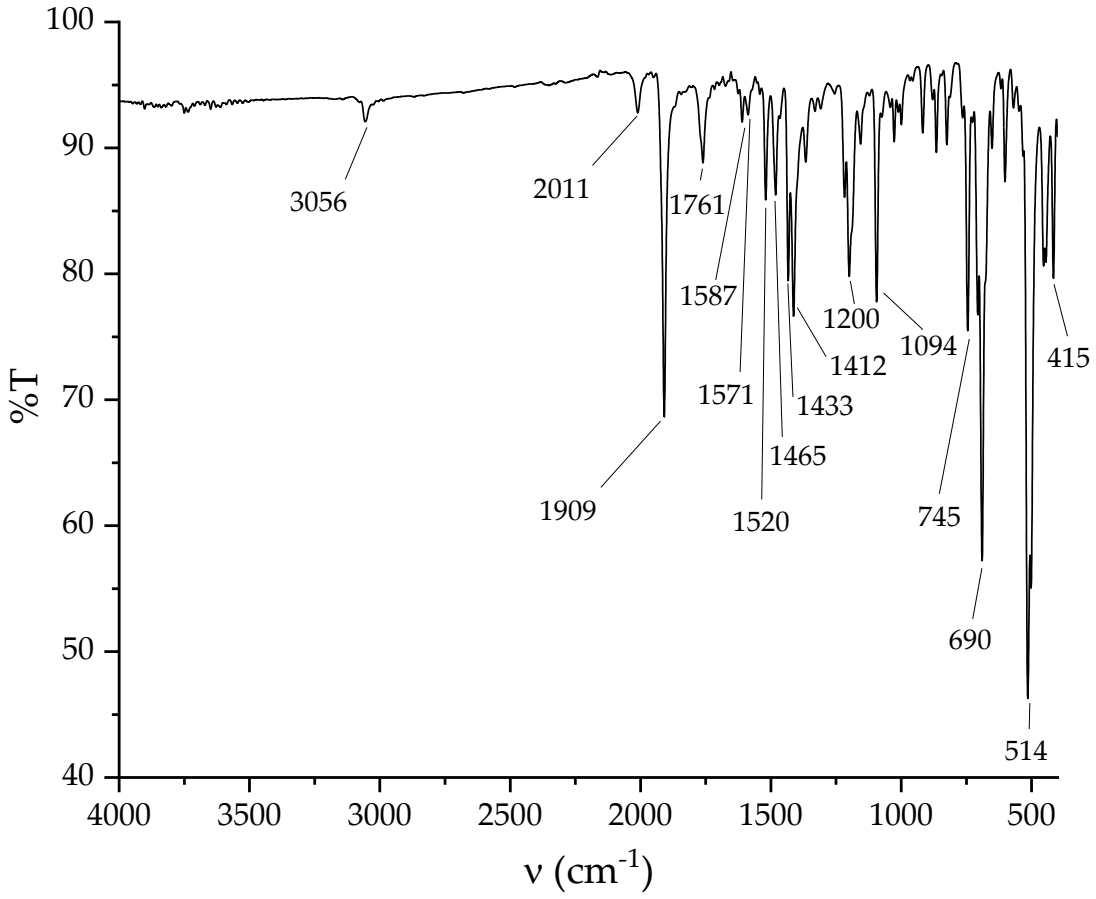

Figure S25. IR spectrum of **5.**

ESI-MS spectrum

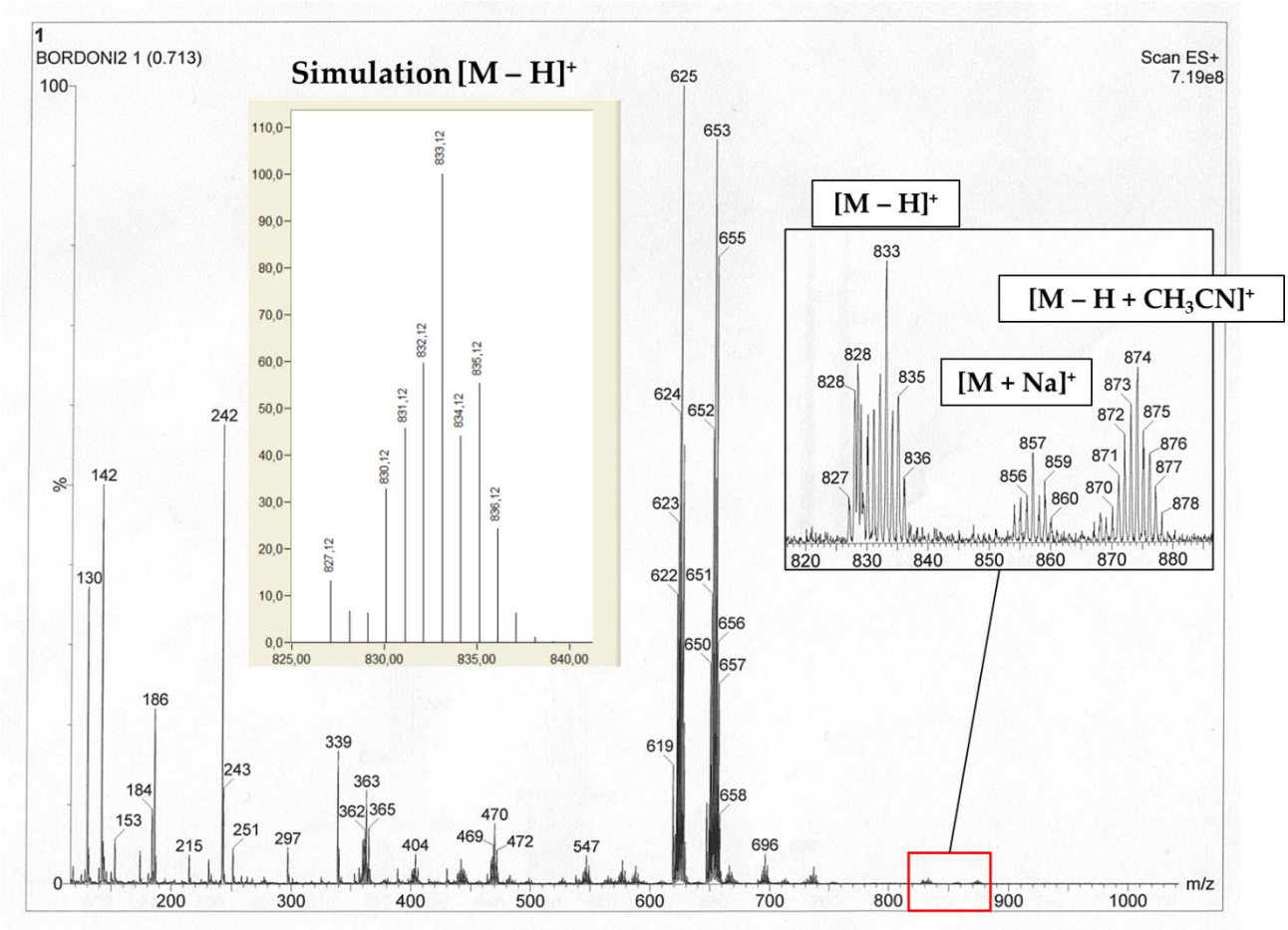

Figure S26. ESI-MS spectrum of **5** compared to simulation (positive mode, CH_3CN).

NMR spectra

^{1}H

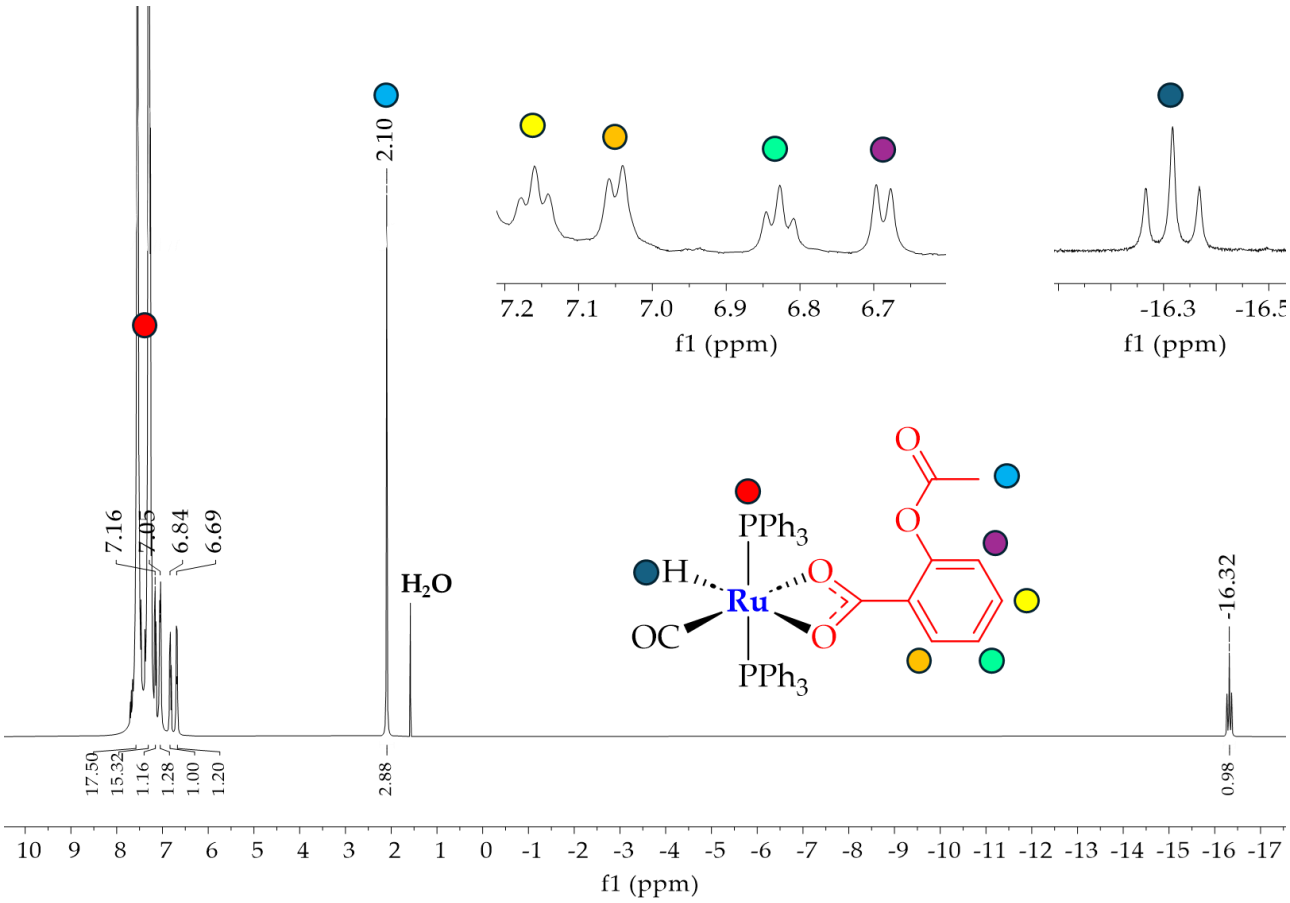

Figure S27. ^{1}H NMR spectrum of **5** ($CDCl_3$).

$^{31}P\{^{1}H\}$

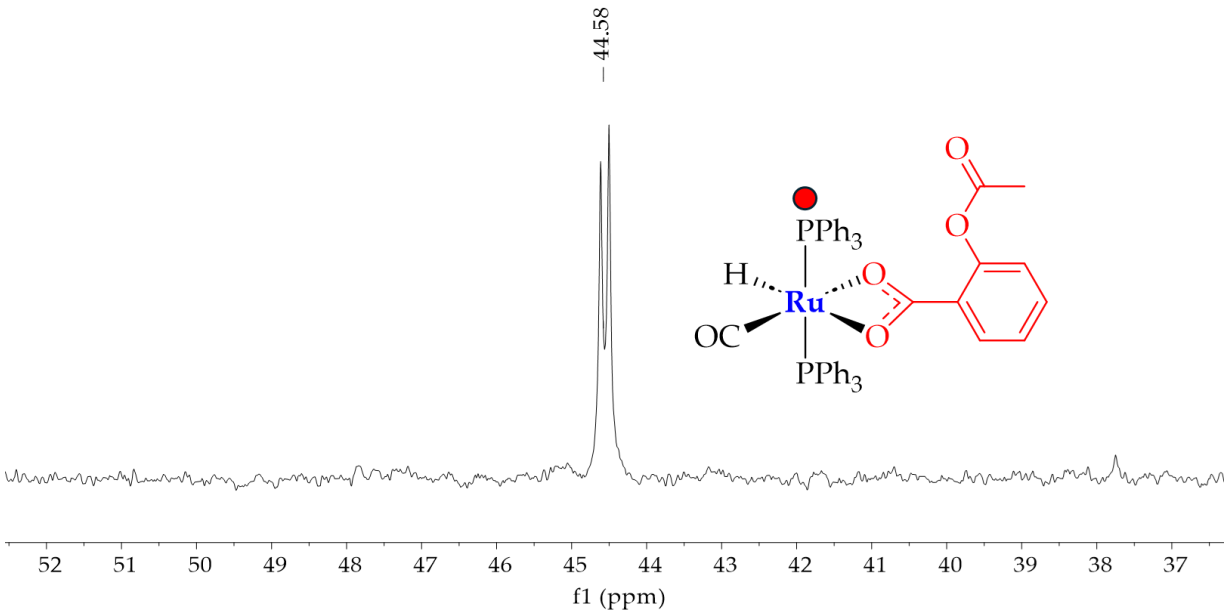

Figure S28. $^{31}P\{^{1}H\}$ NMR spectrum of **5** ($CDCl_3$).

$^{13}C\{^{1}H\}$

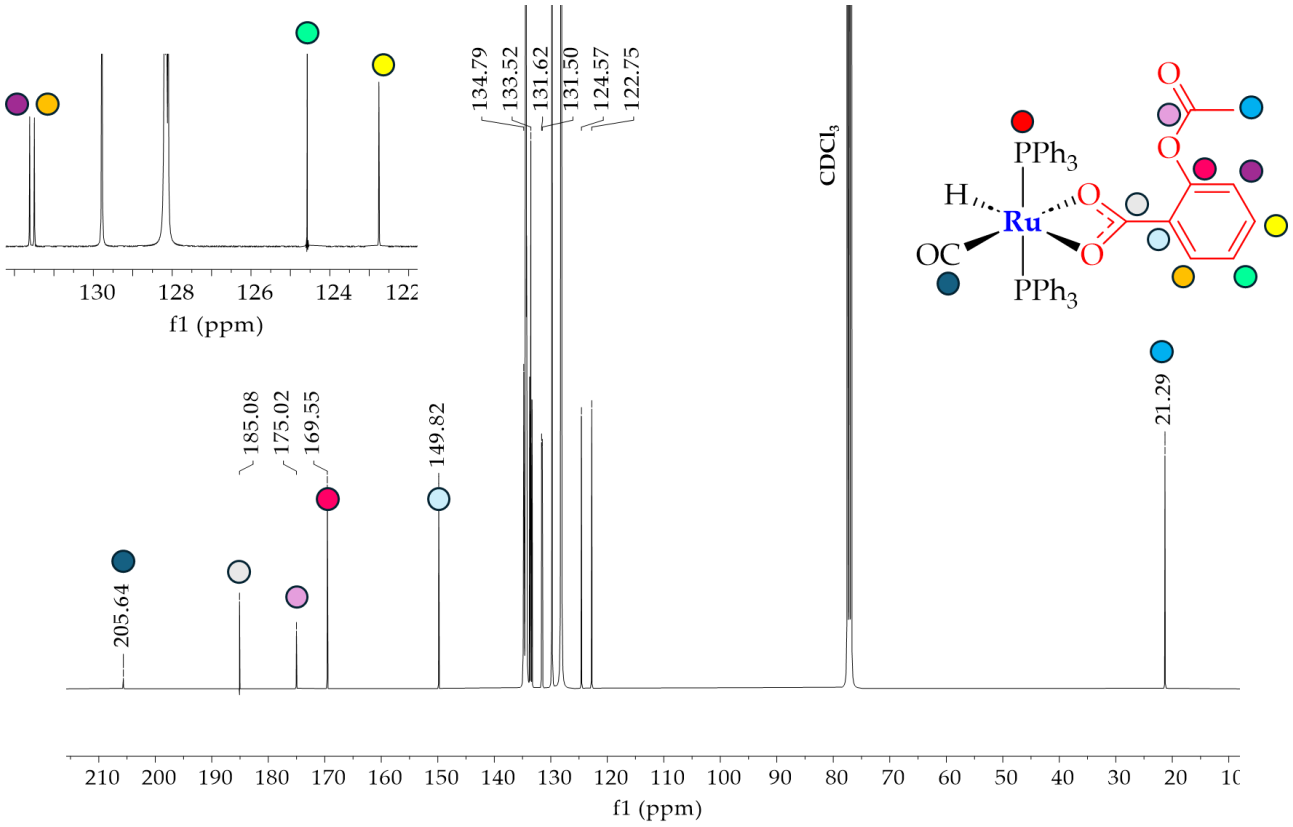

Figure S29. $^{13}C\{^{1}H\}$ NMR spectrum of **5** ($CDCl_3$).

HSQC

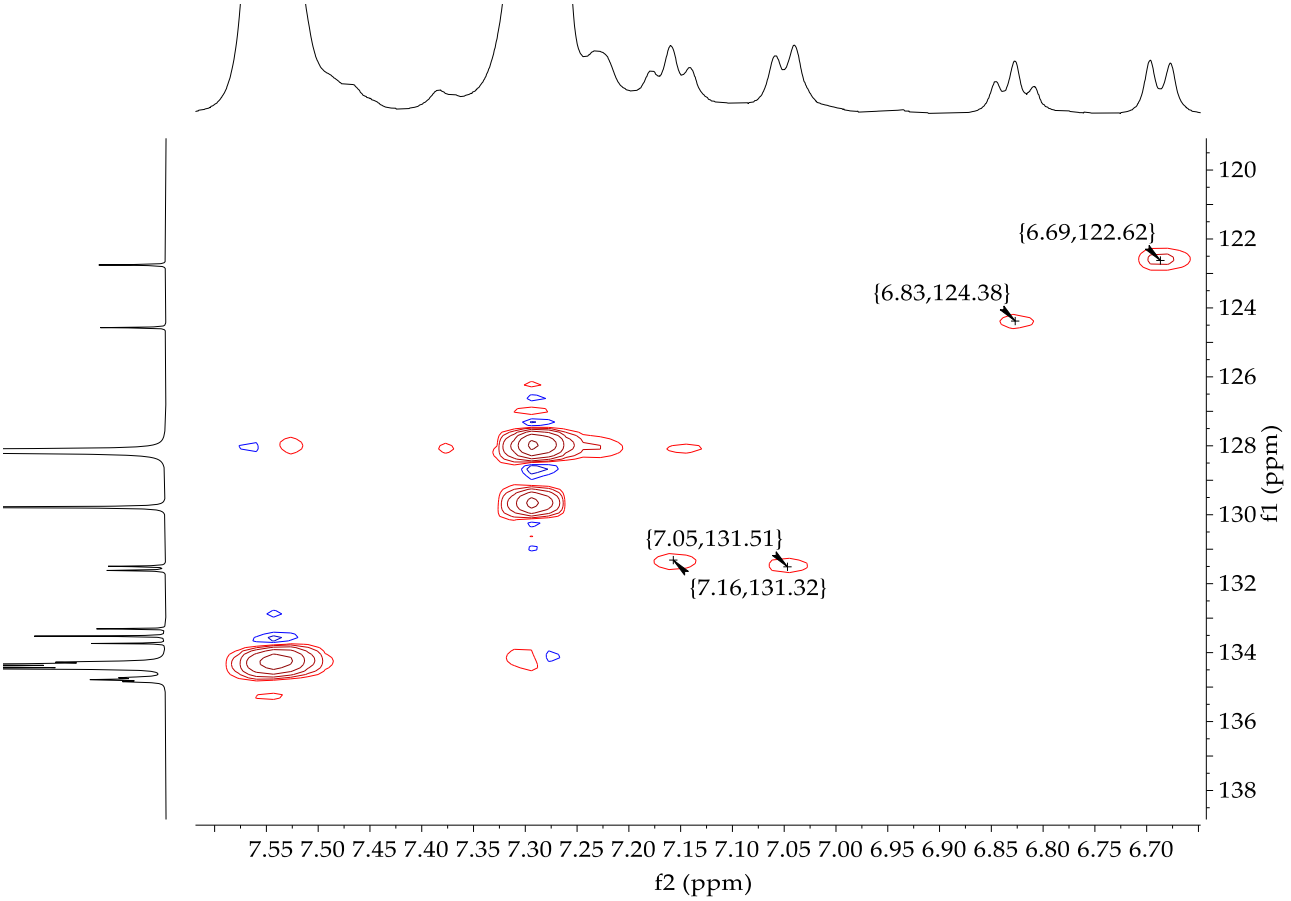

Figure S30. HSQC spectrum of **5** ($CDCl_3$).

HMBC

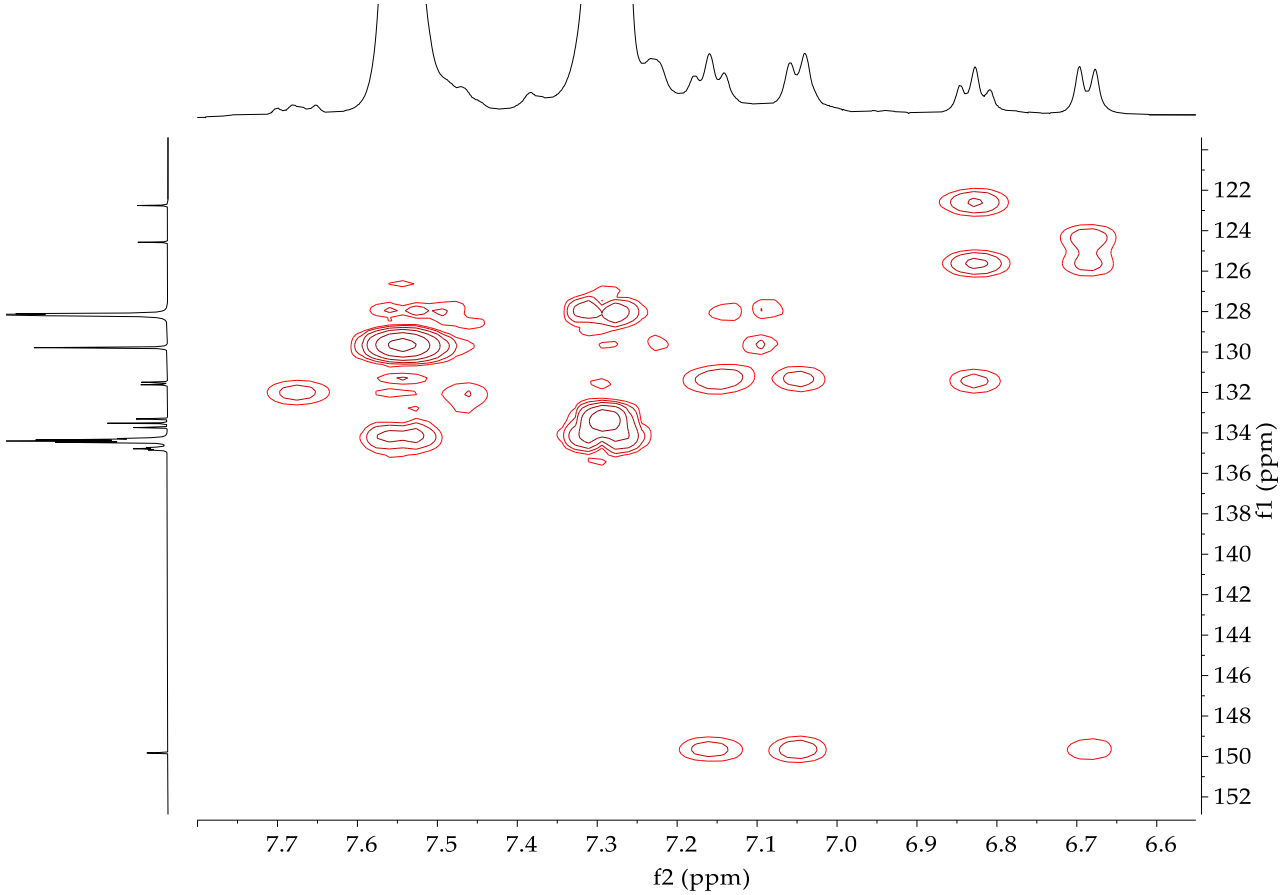

Figure S31. HMBC spectrum of **5** ($CDCl_3$).

UV-Vis spectrum

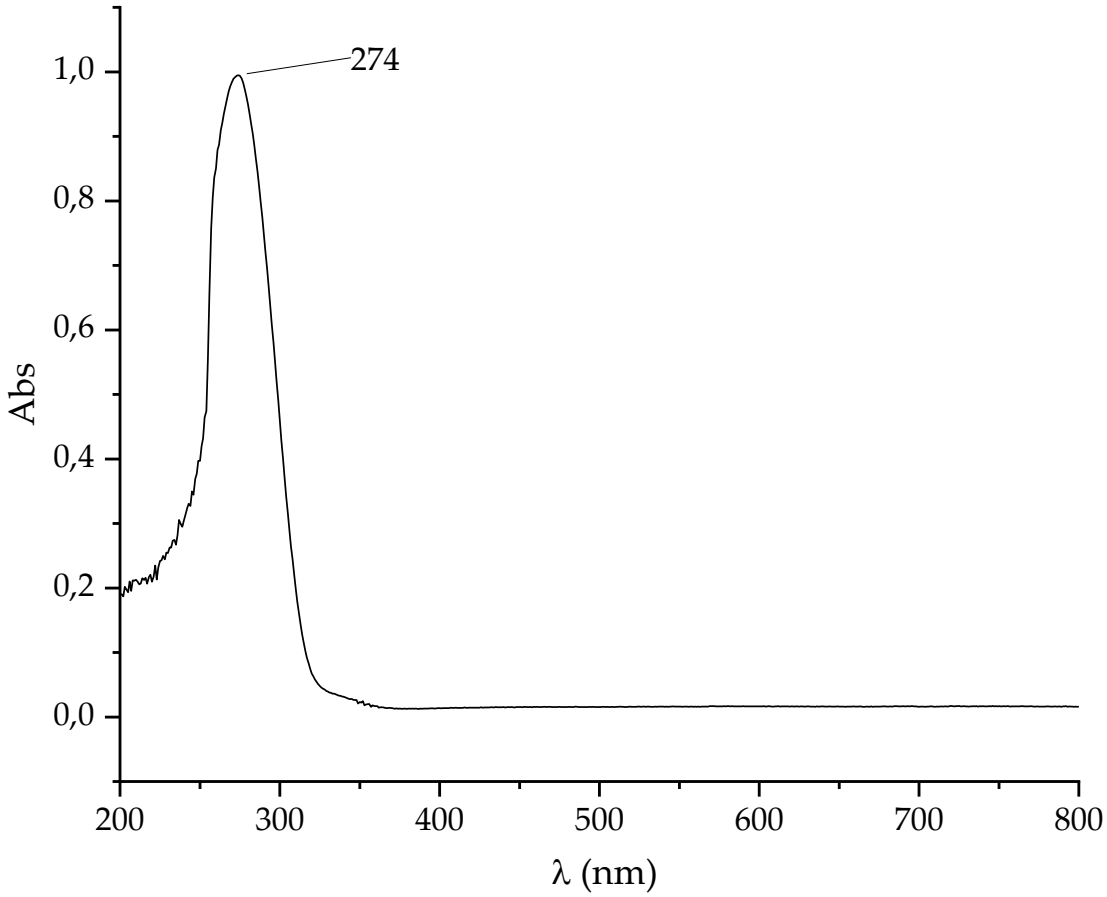

Figure S32. UV-Vis spectrum of **5** ($1x10^{-5}$M, DMSO).

Characterization of **6**

IR spectrum

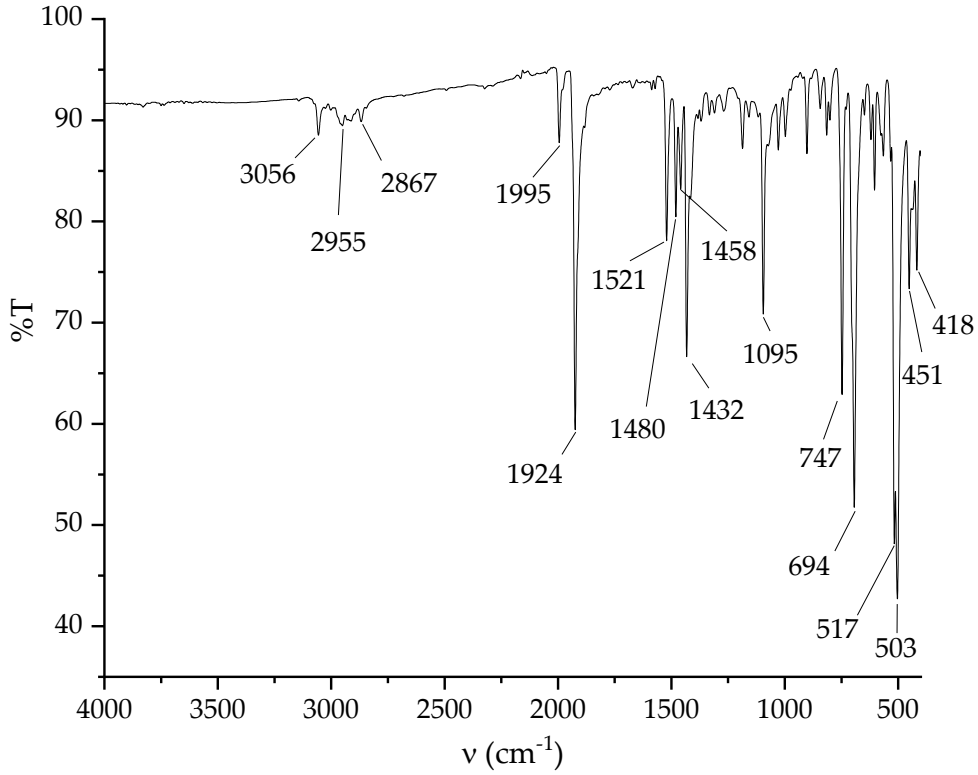

Figure S33. IR spectrum of **6.**

ESI-MS spectrum

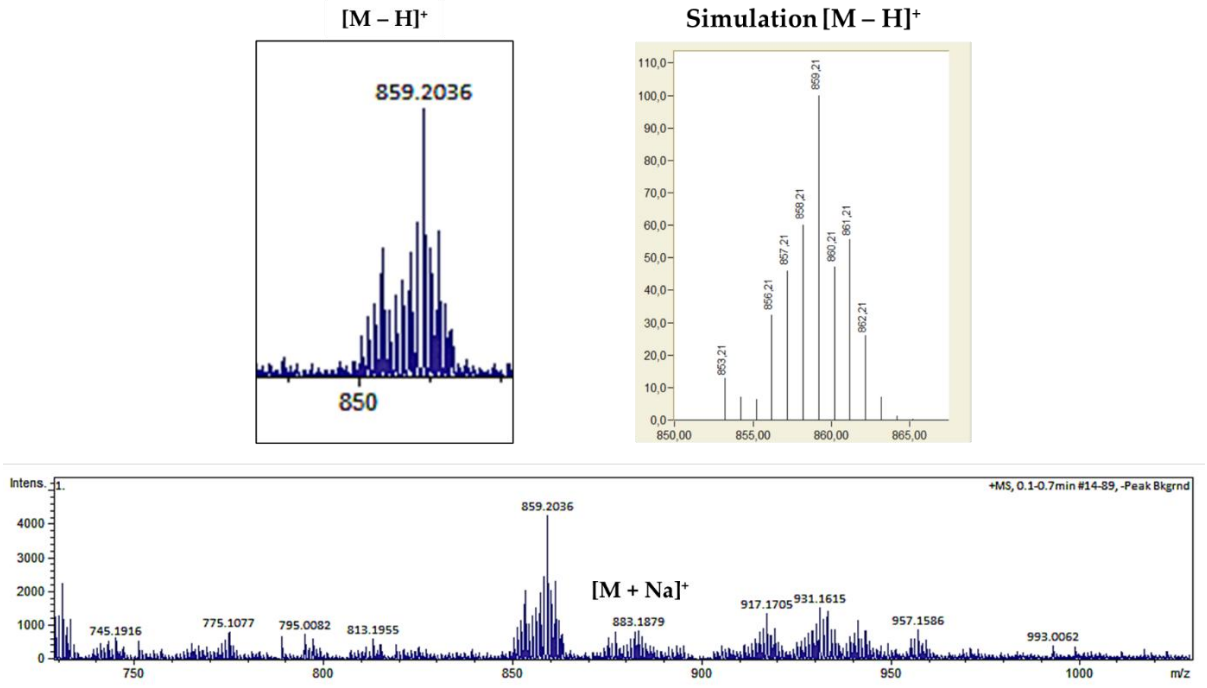

Figure S34. ESI-MS spectrum of **6** (positive mode, CH_3CN).

NMR spectra

^{1}H

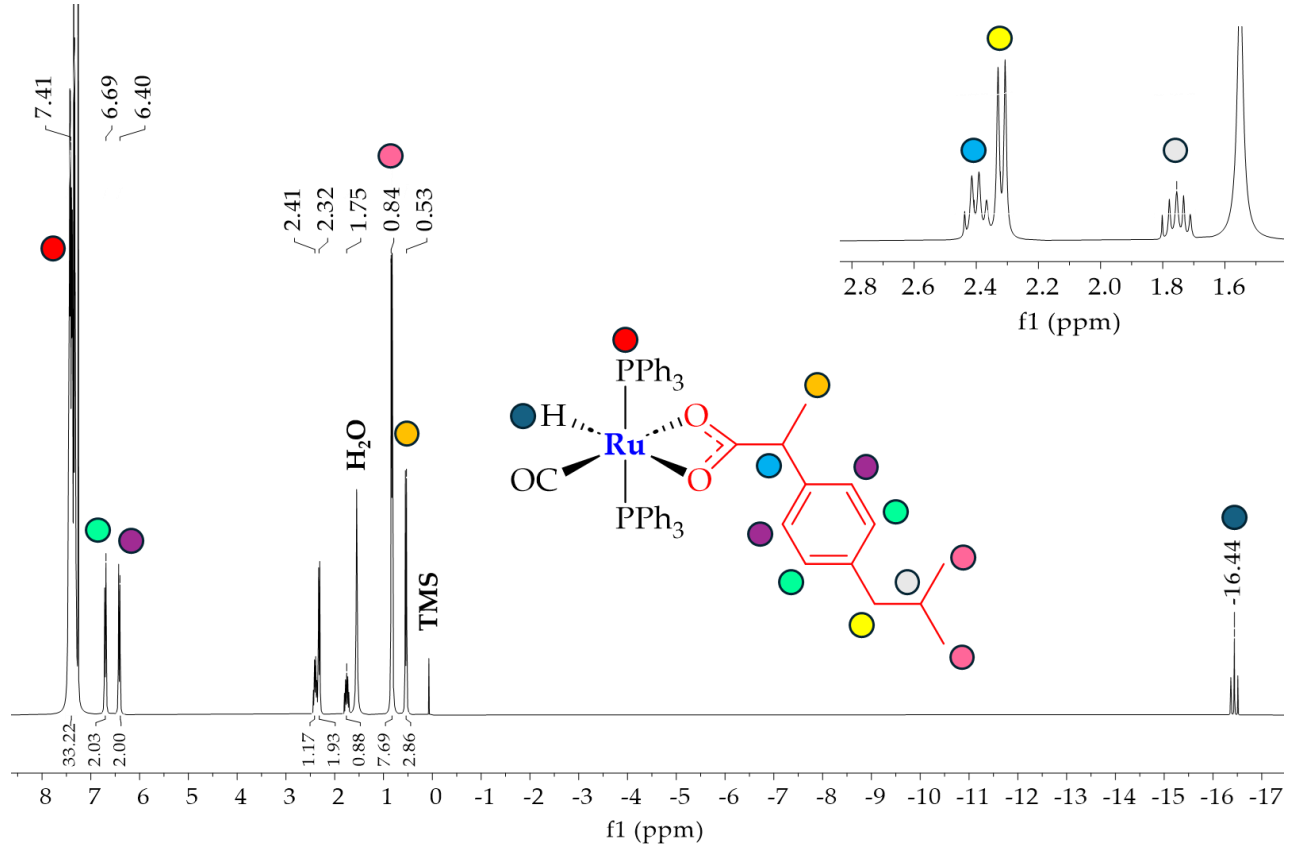

Figure S35. ^{1}H NMR spectrum of **6** ($CDCl_3$).

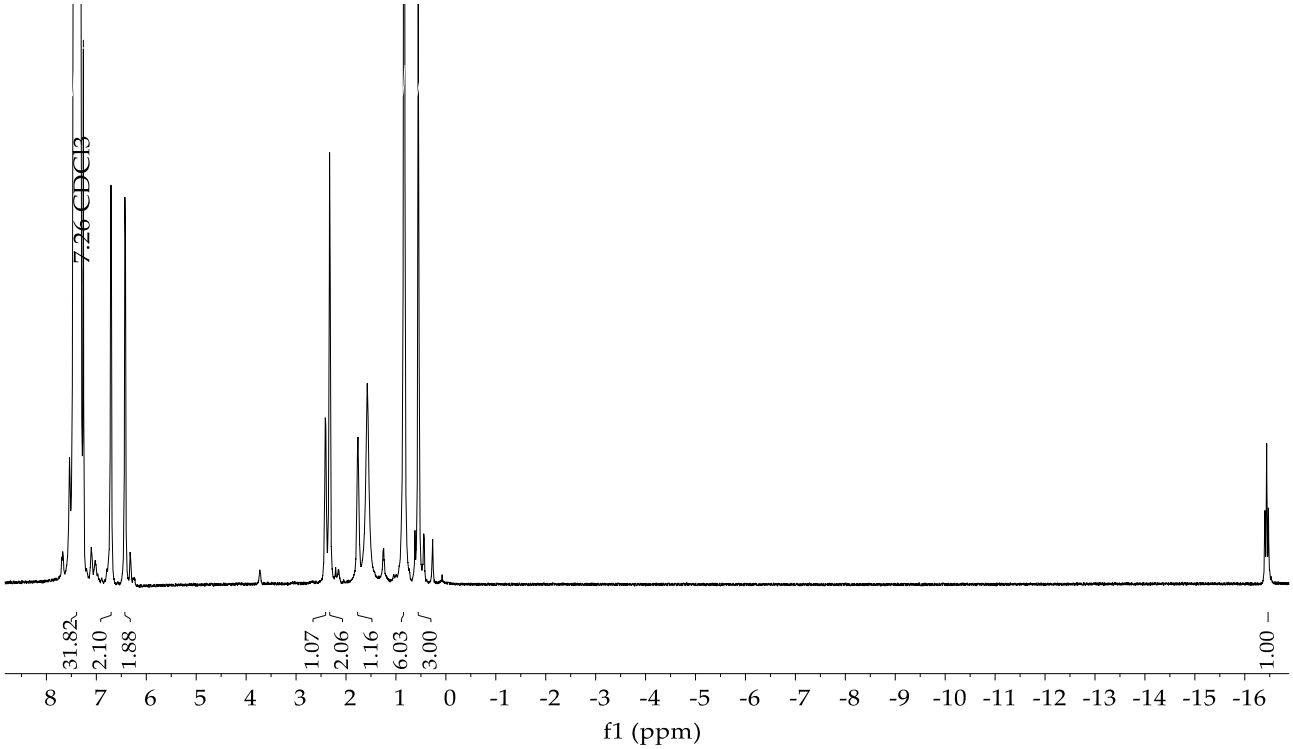

Figure S36 – ^{1}H NMR spectrum of **6** ($CDCl_3$) acquired after 48 h.

$^{31}P\{^{1}H\}$

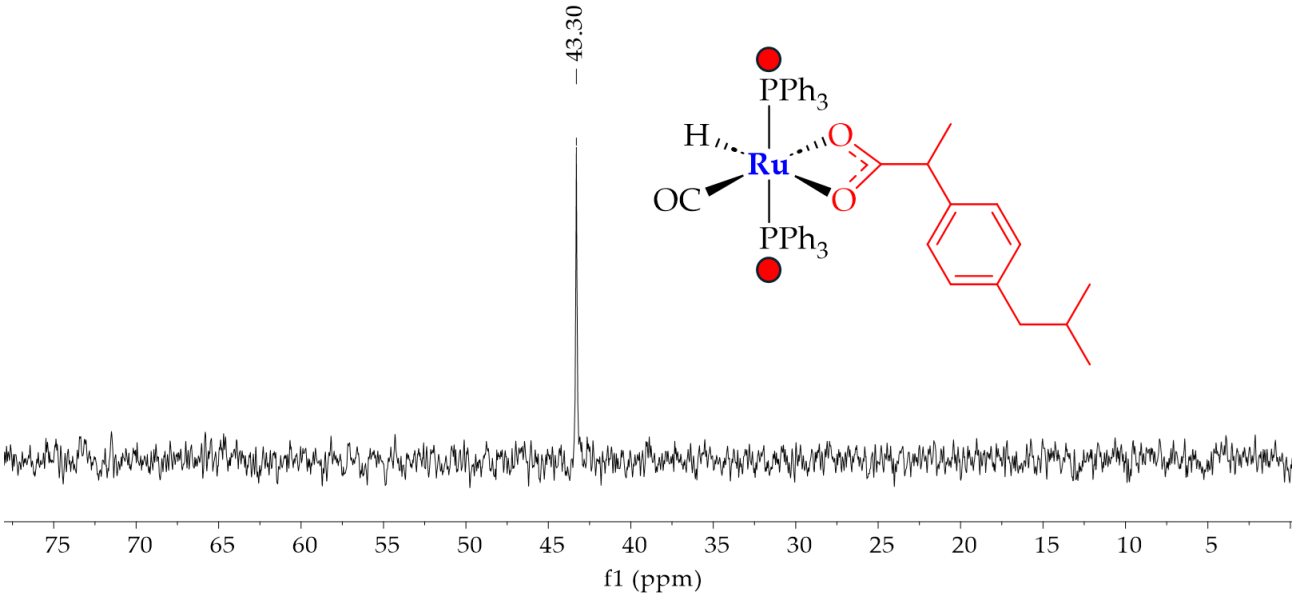

Figure S37. $^{31}P\{^{1}H\}$ NMR spectrum of **6** ($CDCl_3$).

$^{13}C\{^{1}H\}$

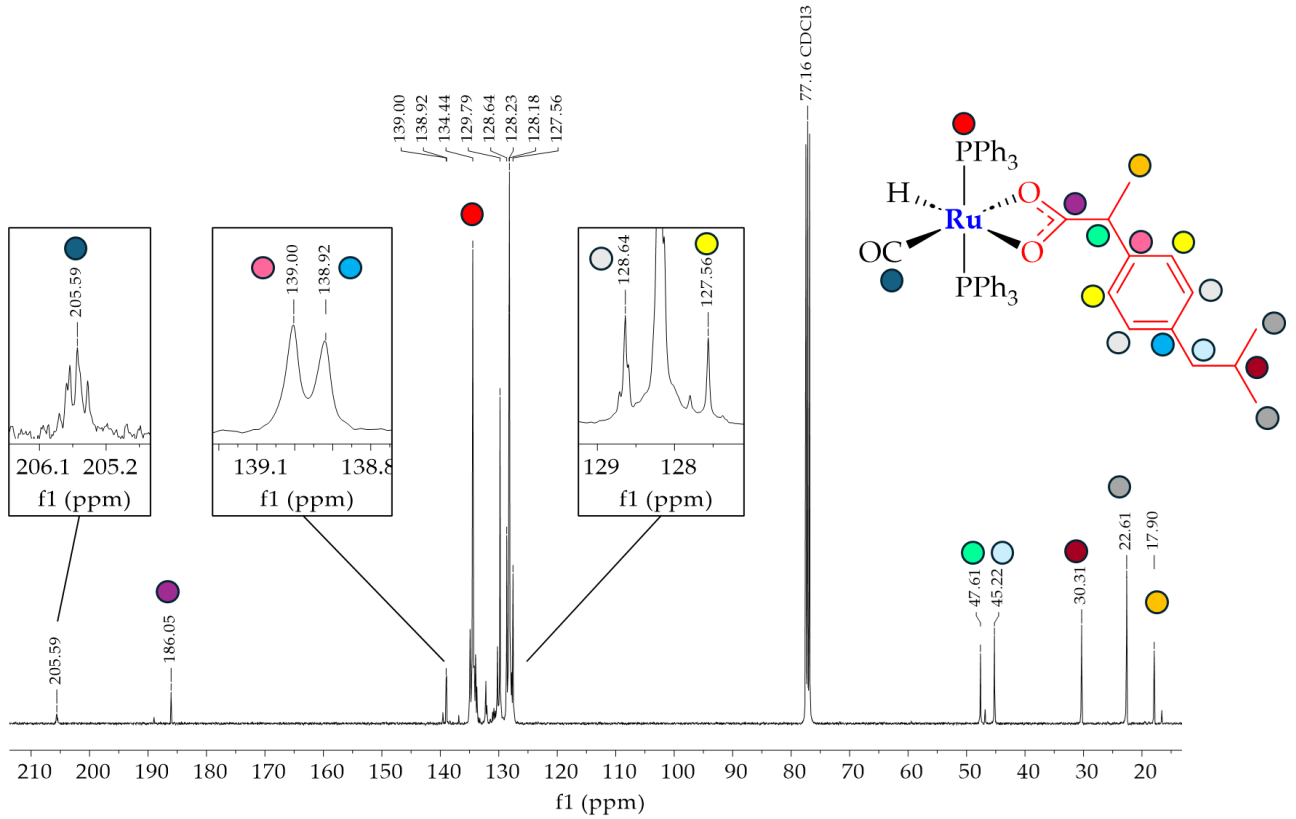

Figure S38. $^{13}C\{^{1}H\}$ NMR spectrum of **6** ($CDCl_3$).

HSQC

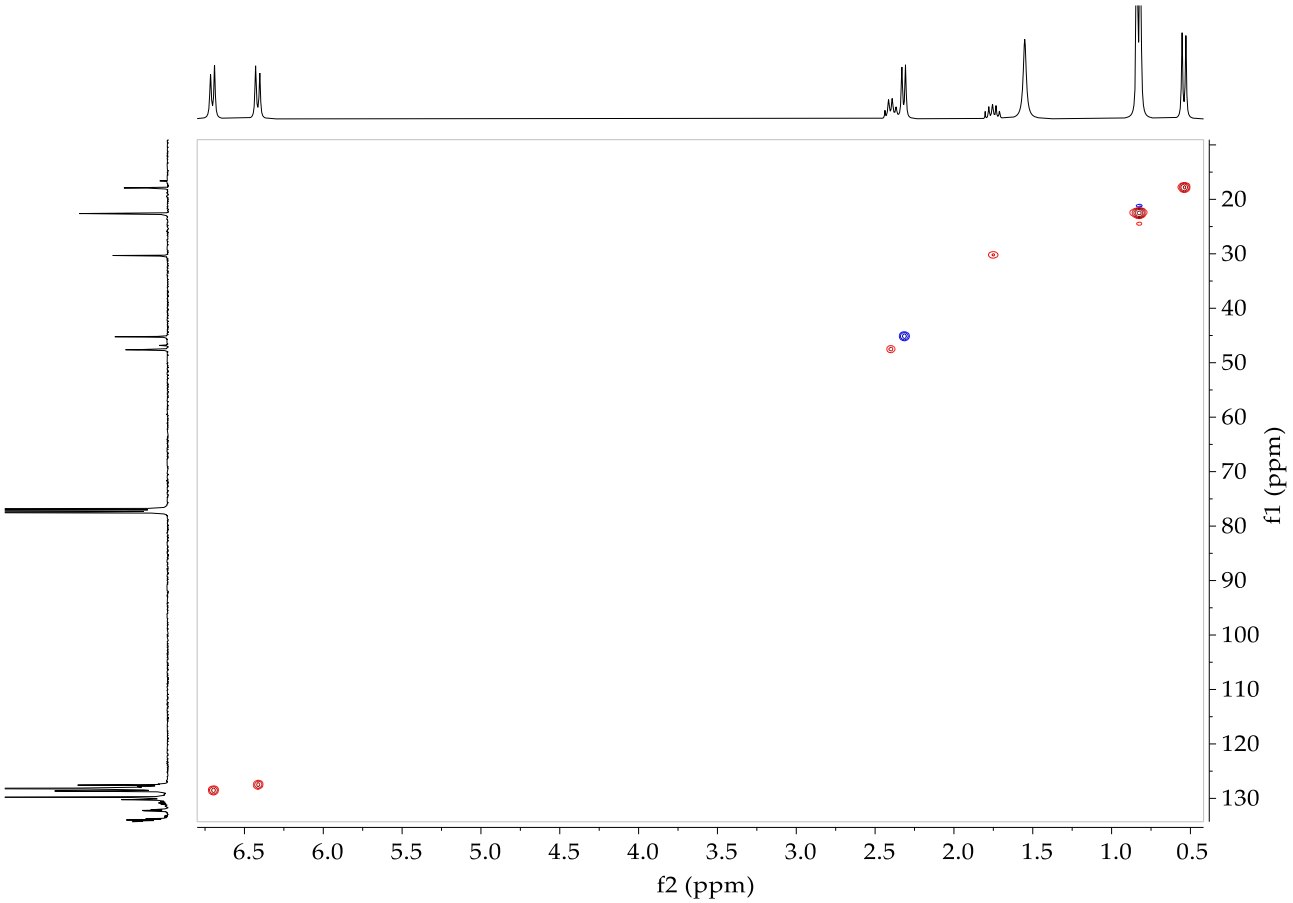

Figure S39. HSQC spectrum of **6** ($CDCl_3$).

HMBC

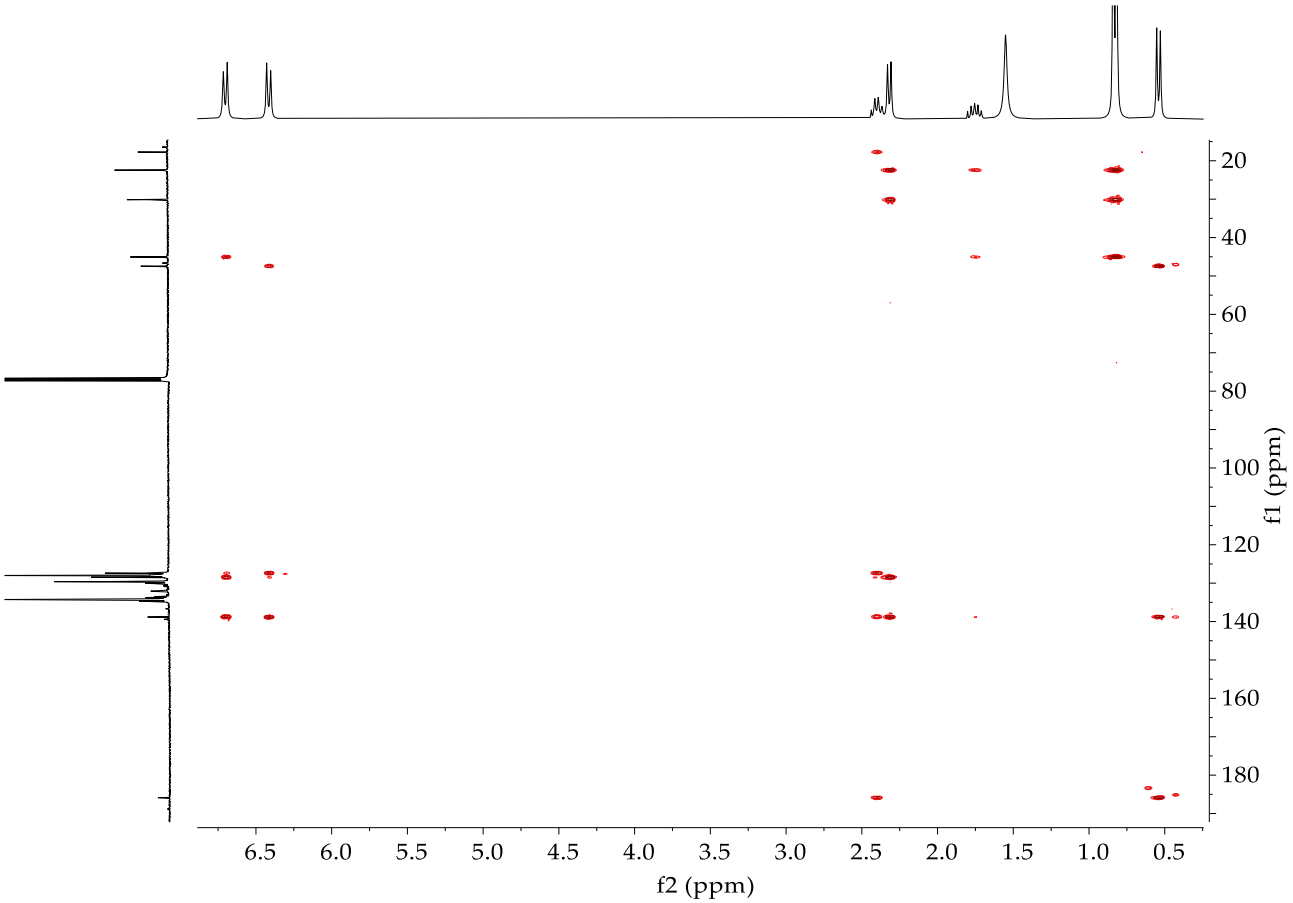

Figure S40. HMBC spectrum of **6** ($CDCl_3$).

UV-Vis spectrum

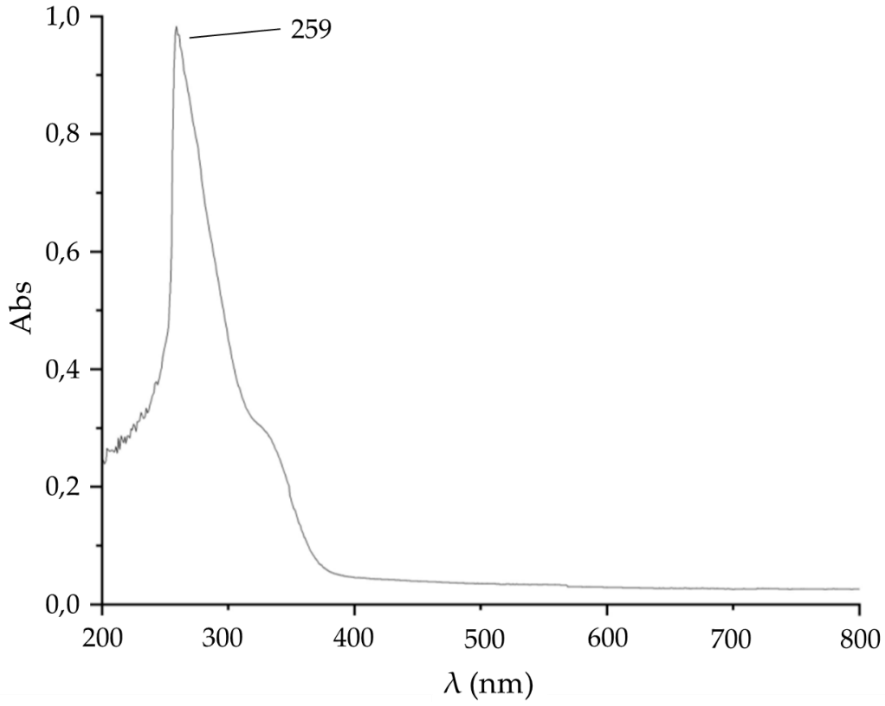

Figure S41. UV-Vis spectrum of **6** ($1x10^{-5}$ M, DMSO).

X-ray diffraction studies

Crystal data

Crystallographic data have been deposited with the Cambridge Crystallographic Data Centre (CCDC) as supplementary publication number CCDC 2496698-2496699 for **4** and **5**, respectively. Copies of the data can be obtained free of charge via www.ccdc.cam.ac.uk/getstructures.

Table S1. Crystal data and experimental details for **4** and **5**.

Compound	**4**	**5**
Formula	$C_{51}H_{41}Cl_2NO_3P_2Ru$	$C_{46}H_{38}O_5P_2Ru$
Fw	949.76	833.77
T, K	296(2)	100(2)
λ, Å	0.71073	1.54178
Crystal symmetry	Triclinic	Orthorhombic
Space group	P-1	Pnma
a, Å	10.1812(3)	10.8580(2)
b, Å	13.9894(4)	22.6928(5)
c, Å	15.8795(5)	15.5452(4)
α, °	86.243(1)	90
β,°	88.276(1)	90
γ, °	89.953(1)	90
Cell volume, Å^3	2255.82(12)	3830.31(15)
Z	2	4
D_c, Mg m^{-3}	1.398	1.446
μ(Mo-K$_\alpha$), mm^{-1}	0.580	4.484 [μ(Cu-K$_\alpha$)]
F(000)	972	1712
Crystal size/ mm	0.16 x 0.09 x 0.05	0.10 x 0.07 x 0.05
θ limits, °	2.001 to 25.999	3.446 to 68.419
Reflections collected	29809	40421
Unique obs. Reflections [$F_o > 4\sigma(F_o)$]	8728 [R(int) = 0.0580	3610 [R(int) = 0.1366]
Goodness-of-fit-on F^2	1.100	1.058
R_1 (F)[a], wR_2 (F^2) [$I > 2\sigma(I)$][b]	0.0451, 0.1078	0.0653, 0.1660
Largest diff. peak and hole, e. Å^{-3}	0.926 and -0.426	0.669 and -0.964

[a])$R_1 = \Sigma||F_o|-|F_c||/\Sigma|F_o|$.[b] $wR_2 = [\Sigma w(F_o^2-F_c^2)^2/\Sigma w(F_o^2)^2]^{1/2}$ where $w = 1/[\sigma^2(F_o^2) + (aP)^2 + bP]$ where $P = (F_o^2 + F_c^2)/3$.

Crystal packing of **4**

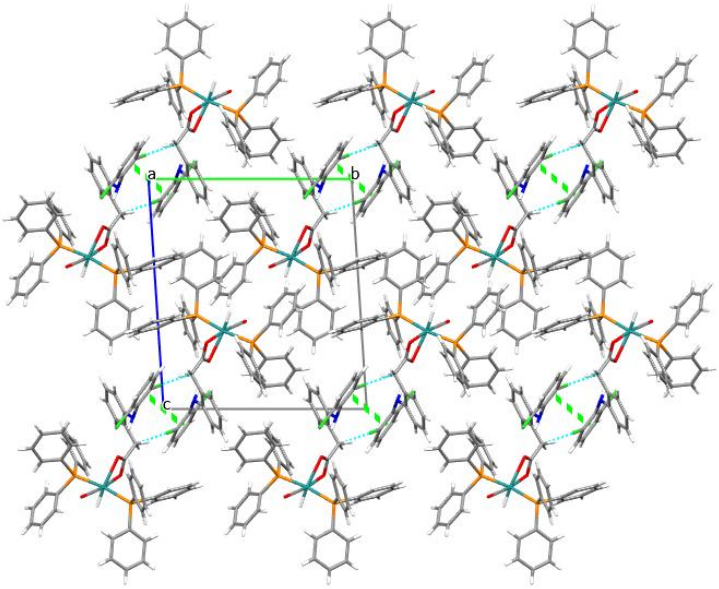

Figure S42. View down the *a* axis of the crystal packing of **4**.

Crystal packing of **5**

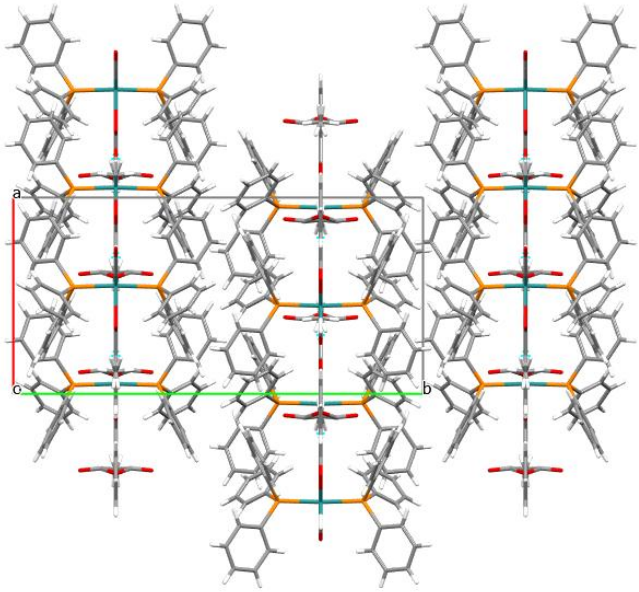

Figure S43. View down the *c* axis of the crystal packing of **5**.